2011

Substrate Integrated Waveguide Horn Slot Antenna Array

Saritha Muguti
University of Mississippi

Substrate Integrated Waveguide Horn Slot Antenna Array

A Thesis

Presented for the

Master of Science

Degree

The University of Mississippi

Saritha Muguti

May 2011

ABSTRACT

Substrate integrated waveguide (SIW) is a rectangular dielectric-filled waveguide, which is synthesized in a planar substrate with arrays of metallic vias to realize bilateral side walls and its transitions with planar structures. These vias act as walls of the waveguide supporting current flow, thus allowing for waveguide mode propagation. Substrate integrated waveguide is suggested for low-loss, low-cost and high density integration applications. SIW preserves the advantages from both the traditional rectangular waveguide and microstrip for easy integration. It is used in designing passive circuits such as resonators, couplers, filters, power dividers, circulators, and antennas

Here, full wave analysis is used to design microwave components such as power dividers, T-junctions and right angle bends. Then a transmission line concept is used to construct a feeding network based on these components to speed up the design process. This concept is verified with full wave analysis. Co-simulation technique is investigated and implemented for the feeding network using these passive components resulting in reduced computation time. The response of the feeding network with the antennas such as an H-plane horn in an array environment is investigated. In the process, modified designs for the H-plane horn with a novel concept of a slot on the H-plane horn are achieved and used as elements for the linear arrays.

DEDICATION

This work is dedicated to my parents.

Without their support, I would never be where I am.

TABLE OF CONTENTS

LIST OF FIGURES

FIGURE **PAGE**

CHAPTER I

Introduction

With the rapid development of modern wireless communication, high integration and minimization of circuits has been demanded [1]-[4]. Substrate Integrated Waveguide (SIW) is an attractive guided-wave structure, for low loss, low cost and high density integration of microwave and millimeter wave components. This approach combines both the advantages of the microstrip lines and waveguide, and has shown its promising future [5]. The SIW has provided a very useful technology for the implementation of filters and feeding lines for antennas. A number of devices are implemented using SIWs, such as bend and T-structures, six port junctions, oscillators, and waveguide slot array antennas [6-7]. The concept can be used to synthesize many kinds of dielectric based waveguides using metallic vias, most of these structures can be interconnected to planar circuits with simple transitions and fabricated on the same dielectric substrate [1].

The goal of this study is to design and analyze the characteristics of the SIW horn antenna, and also to study the antenna in the array environment. The equivalence between the SIW and conventional rectangular waveguide with an example are elaborated in chapter 2. The feeding network and the description of the components used in the construction of the feeding network are presented in the chapter 3. Also, the comparison of s-parameters for the feeding network, synthesized using code and HFSS simulation software are described in the chapter 3. Feeding network using metallic vias and Feeding network using metallic solid walls are designed

and concluded that the feeding network modeled with the solid walls takes less time in comparison with the metallic vias.

Chapter 4 deals with the different cases of the SIW horn antenna. The issues with the SIW horn antenna due to the presence of discontinuity at the aperture, the possibilities such as dielectric load and slot used to overcome the discontinuity are elaborated. SIW horn with slot on the single surface of the horn without disturbing the PEC, slot on the two sides of the horn are analyzed. SIW horn using two kinds of excitations, rectangular waveguide and coaxial cable are analyzed, the comparison for both the cases are discussed.

The behavior of the SIW modified horn slot antenna in the array environment is described in chapter 5. Initially we started with 4 elements and concluded with 8 elements. The conclusions of this work and the scope for future work are outlined in chapter 6.

CHAPTER II

In microwave circuits and antennas, power dividers and feeding networks are important parts of a system and play a crucial role in their system performance. For microwave or millimeter frequency applications, microstrip type of feeding network has been widely used because of its compact size and easy integration. However, microstrip has high losses and as an open structure produces unwanted radiations. The radiation not only introduces losses but also has a negative impact on the surrounding components. As a conclusion it can be said that the microstrip type of feeding network may not be desirable for higher frequencies because of its high radiation loss and low power capacity [8]. Instead, the waveguide type of feeding network is commonly adopted due to its high performance.

Waveguides are closed structures which can guide electromagnetic (EM) waves along the axial direction and bound all the electromagnetic energy inside the walls, resulting in no radiation loss. Thus, rectangular waveguide is considered as one of the most prominent guiding structures and has been widely used in millimeter-wave systems. However, they are voluminous in nature and expensive for manufacture. Thus, their relative high cost and difficult integration prevent them from being used in low-cost high-volume applications [1]. In the process of fixing these problems a new type of transmission line called substrate

integrated waveguide (SIW) has been proposed. SIW preserves the advantages from both the traditional microstrip for easy integration and the waveguide for no radiation loss [8]. It can be used in designing passive circuits such as resonators, couplers, filters, power dividers, circulators and antennas. This kind of transmission line can be extended to synthesize almost all kinds of dielectric filled waveguide using metallic vias.

2.1 Substrate Integrated Waveguide (SIW)

SIW, also called "post-wall waveguide or laminated waveguide," is a low cost realization of waveguide circuits for millimeter-wave and terahertz applications. It is a type of rectangular dielectric-filled waveguide that is synthesized in a planar substrate with arrays of metallic vias and are designed and integrated on the same substrate [9].

In an SIW circuit, metallic vias are embedded in a dielectric substrate, which is covered with conducting sheets on the top and the bottom, to emulate the vertical walls of a traditional waveguide. It preserves the advantages of the traditional rectangular waveguide circuit, such as low radiation loss, high Q-factor and high power capacity, etc., and it can also be fabricated easily with the existing technologies and also manufactured easily [4]. These SIW circuits are designed to only support TE_{10} mode in the whole operating frequency band.

2.2 SIW Design Rule

For the construction of an SIW, the rectangular waveguide is synthesized by placing two rows of metallic vias in the substrate, as shown in Figure.2.1 The physical dimensions, such as the diameter **D** of the vias, the spacing **b** between the vias, and the spacing **a** between the two rows of vias, play a vital role in constructing an SIW. The spacing **b** between the vias

must be kept small to reduce the leakage loss between the adjacent posts. Thus, the spacing **b** and the post diameter **D** are interrelated.

In order to neglect the radiation loss between the adjacent posts, two design rules corresponding to the post diameter **D** and separation distance **b** are used and these rules have been concluded from the simulation results of different SIW geometries [9].

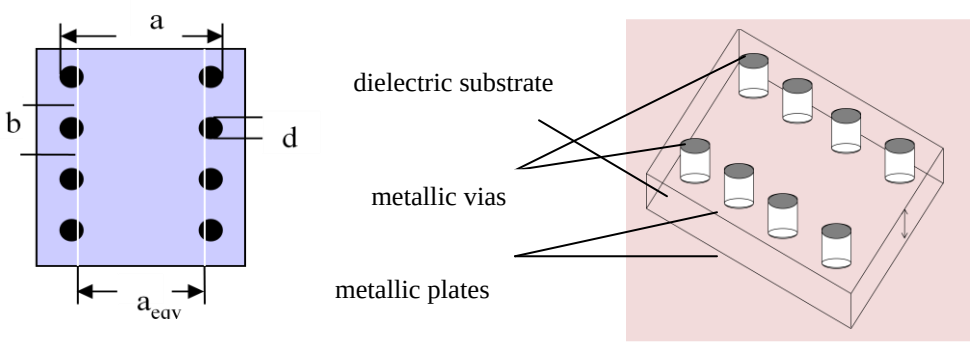

Figure 2.1 SIW Structure (a) Top view and (b) Side view

The two design rules are:

1. the diameter **D** has to be less than one fifth of the guided wavelength

   $\mathbf{D < \lambda_g/5}$

2. the spacing **b**, between the vias (center to center) must be less than or equal to twice the diameter:

   $\mathbf{b \leq 2D}$

These rules have to be satisfied to reduce the leakage loss but not always necessary; a diameter **D** larger than one fifth of guided wavelength or spacing between the vias **b** larger than two diameters can also be used but with more care. But these two rules ensure that the radiation loss will be negligible.

2.3 Equivalence between SIW and Conventional Waveguide:

In order to understand the equivalence between the SIW and rectangular waveguide as shown in Figure 2.2, we have examined an SIW structure having 5 metallic vias in each row which are embedded in a dielectric substrate and covered with conducting sheets on the top and the bottom as shown in Figure 2.3.

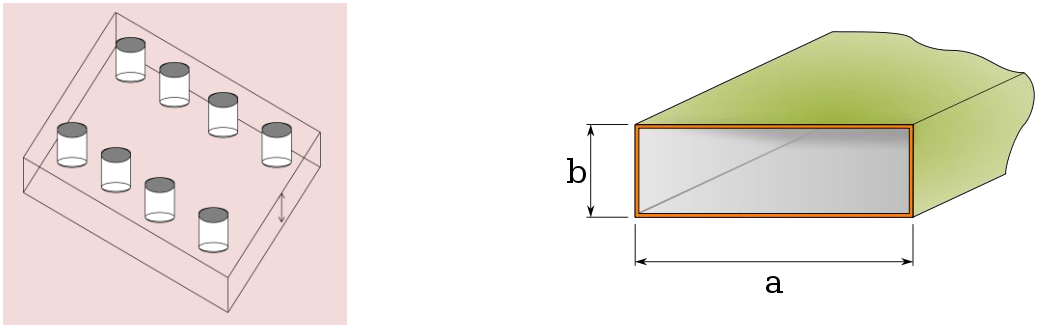

Figure 2.2 Substrate integrated waveguide (SIW) and Conventional rectangular waveguide

This example has been modeled using the simulation software HFSS to observe the fields in the waveguide and is excited using a wave port at the operating frequency.

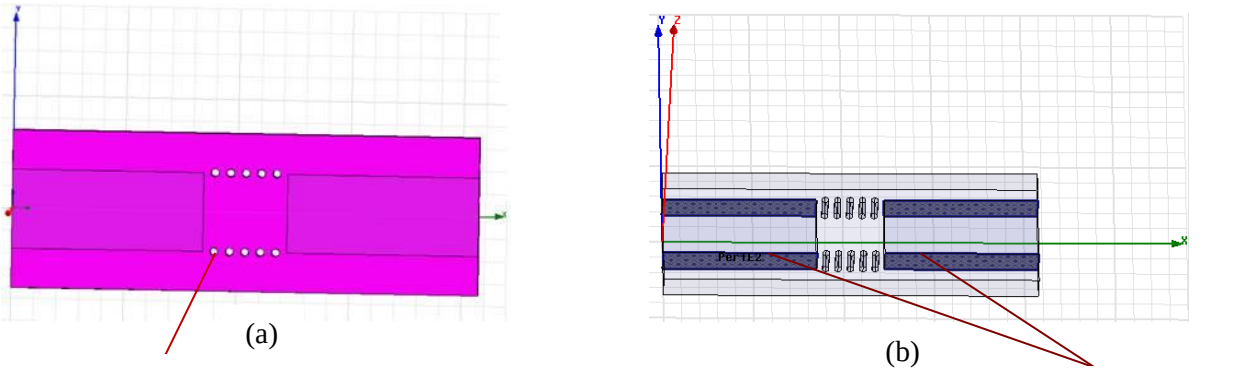

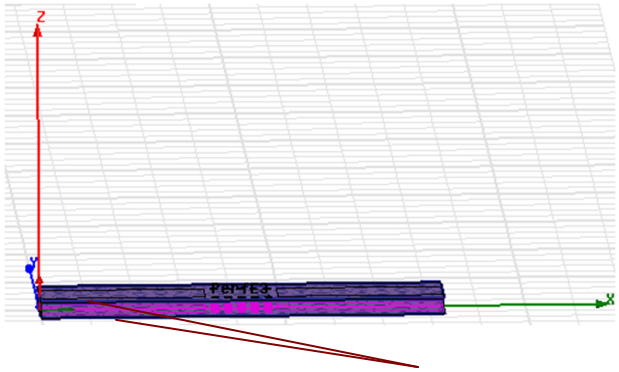

(c)

Metallic sheets

Diameter of the vias (d) = 0.775 mm

Spacing between the vias (b) = 1.3725 mm

Spacing between the two rows (a) = 7 mm

Height of the substrate (h) = 3.175 mm

Permittivity of the substrate (εr) = 2.2

Figure.2.3 SIW waveguide (a) Top view, (b) Another view and (c) Geometry

It can also be observed that a PEC boundary condition is assigned on the walls of the partial waveguide which makes sure that the electromagnetic waves are bounded between these two walls. The electric field distribution and reflection coefficient for this structure are shown in Figure. 2.4.

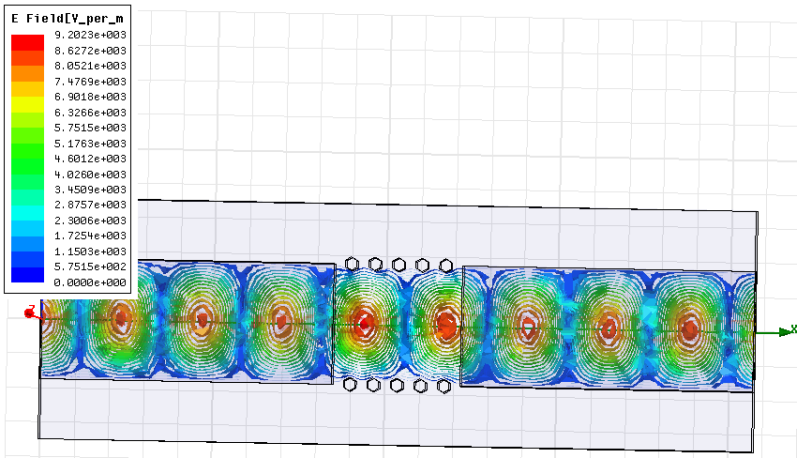

(a)

(b)

Height of the substrate (h) = 3.175 mm

Permittivity of the substrate (εr) = 2.2

SIW equivalent port width a_{eq} = 7.3 mm

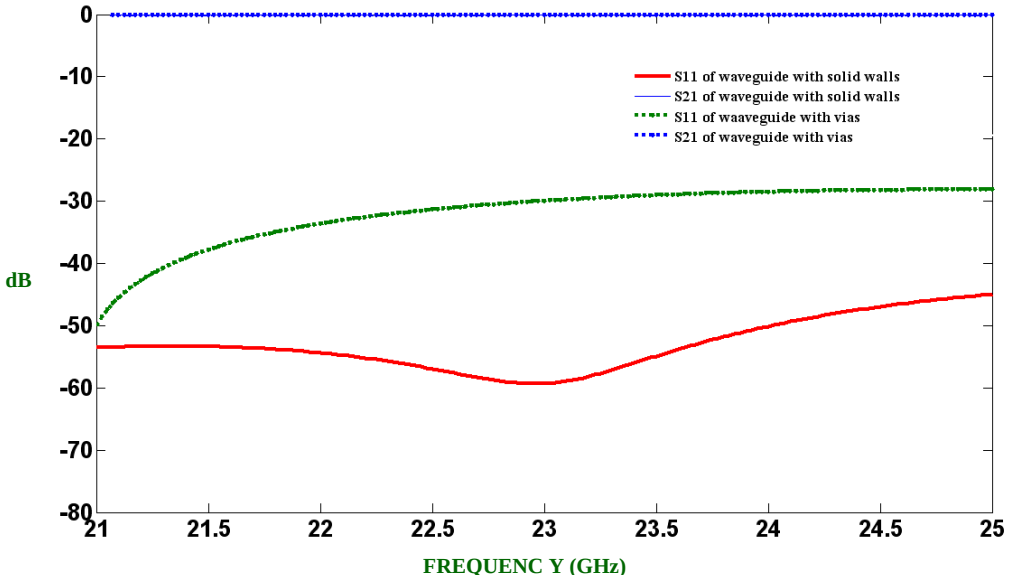

(c)

Figure 2.4 SIW Waveguide Circuit (a) Electric Field Distribution, (b) Waveguide with metallic solid walls and (c) Reflection coefficient

Figure 2.4 (a) shows that there is no leakage of power from between the metallic vias and the vias are acting as the solid walls. It has been observed that as the number of metallic vias increases, the computation time for the analysis of the SIW circuits increases. Since the waveguide geometry shown in Figure 2.3 (a) consists of 10 vias, the computation time is negligible. However, the computation time for the SIW structures such as filters, power dividers, directional couplers, etc., will be high as the geometry may consists of hundreds of vias,. In order to fix this problem we have tried to replace metallic vias with metallic solid walls with respect to the SIW equivalence which is explained later as shown in Figure.2.4 (b). The S-parameters for the SIW waveguide which is modeled using metallic vias and the waveguide modeled using solid walls is shown in Figure 2.4 (c). In both the cases a good matching is observed, which is below 30 dB.

By comparing the SIW and its equivalent rectangular waveguide, we find that they both have the same shorter dimension **h** and the longer dimension **a.** The SIW equivalent port width ($\mathbf{a_{eqv}}$), used in modeling the waveguide using solid walls is computed using the following equation:

$$a_{eqv} = a - D - \frac{D^2}{0.95 \times b}$$

This equation is a function of the distance between the two lines of vias that form the side walls **a,** the separation between these vias **b** and diameter of the vias **D** [1]**.**

Table.1.1 Comparison of Simulation Time for a Waveguide

	waveguide with the metallic vias	waveguide with the solid walls
simulation time (minutes)	28	4

2.4 Solution for an SIW:

In order to study a general substrate integrated waveguide circuit, a full wave analysis is required. If we consider the circuit as a 2D problem assuming no field variation normal to the substrate, with only vertical electric and horizontal magnetic fields and placed in a horizontal plane, Finite Element Method and FDTD can be used to solve the problem, but they require the geometry discretization of the entire circuit which may require large memory and might be time consuming.

Method of moments (MOM), which discretizes the geometry discontinuities may also be used. However, the thin wire approximation which assumes constant current density may be invalid for a metal post (metallic via) on the post wall even if it is electrically thin, because the field strength inside the guide is much stronger than that outside the circuit. Thus, the discretization of the metal posts cannot be avoided, which increases the system matrix size. Also, in MOM, the boundary condition is enforced at discrete positions on a metal post if point matching is adopted, or at the entire surface in an average sense if a testing procedure is applied. Recently a Hybrid Method, which is a combination of MOM and cylindrical

eigenfunction expansion, was introduced [4]. This method is only applicable for the non-radiating structures.

In the Hybrid Method the field due to a cylinder can be written in a series of cylindrical eigenfunctions, whereas the waveguide ports are treated in an MOM manner and a C++ code has been developed for this hybrid method. There is no geometry discretization for the metallic vias, and the boundary conditions over the entire surface of a cylinder can be enforced. Figure 2.5 shows an example of an SIW 1:2 power divider, which is solved using this code.

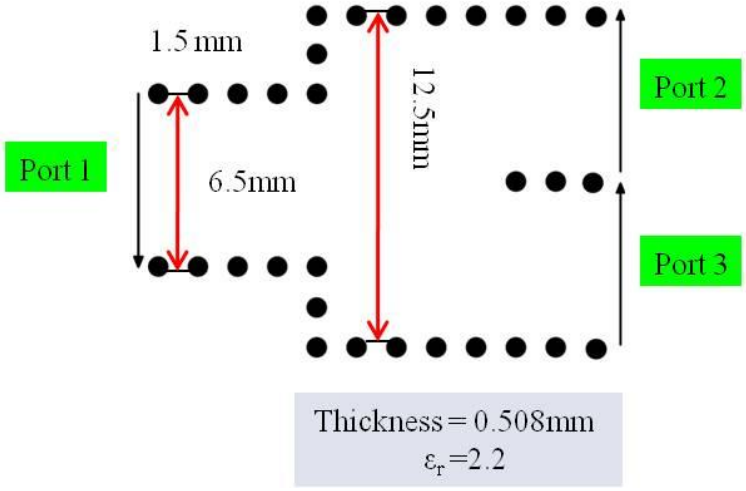

Figure.2.5 Topology of the H-Plane SIW 1:2 power divider

A Y-junction straight structure is adopted for the design of the SIW 1:2 power divider, and the power division section consists of a bifurcated waveguide junction fed by a symmetrical step junction. The distance L between the two discontinuities and the input port width **a** as shown in Figure 2.5, can be optimized to achieve the power division and input specifications as required [8]. The reflection coefficient for this structure is shown in Figure 2.6.

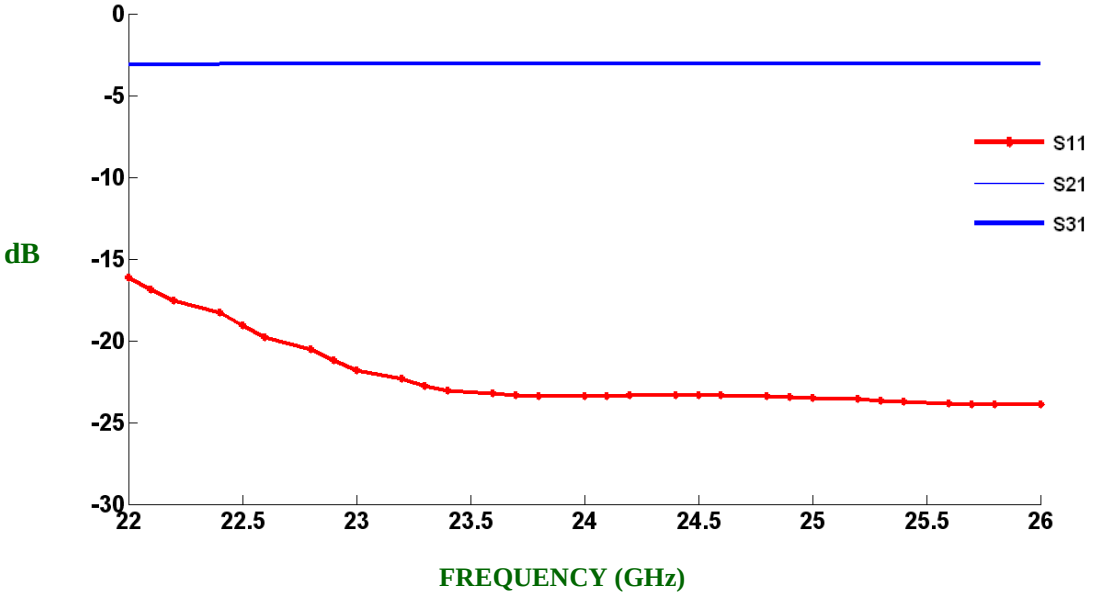

Figure.2.6 Reflection coefficient of the SIW 1:2 power divider

Thus, a 1:2 power divider using the C++ code has been studied and this code can also be extended to design many other passive devices such as directional couplers, circulators, filters, etc. In this work, we have used this code to design the feed of the array and is compared with Finite Element Simulation software [HFSS] , which is discussed in chapter 2.

CHAPTER III

3.1 Feed of the Array

Antenna arrays have wide application. Generally, arrays require power dividers/combiners to divide/combine the input/output power in amplitude and phase to/from the different radiating elements. The divider network should also result in high isolation between the elements and a good impedance match at each port. The difficulty with the feed network is that it depends on the number of elements, the amplitude and/or phase distribution between the elements, and the ability to do beam steering. In most of the array applications bandwidth is a crucial factor in their performance. However, for large arrays, because of the required long transmission lines and the consecutive subarraying, the feed network may be the dominant limiting factor for the bandwidth and it may severely affect the performance where as for small arrays, feed network may not be the dominant limiting factor for the bandwidth [10]. It is important to realize that the feed network is the most complex part of the array.

In this work, the transmission line concept is used to construct the feeding network of the antenna array [12]. Here we use an example of an array of 8 uniformly distributed antenna elements having one input port and eight output ports. The feeding network has been constructed using three fundamental modules: SIW T-type two-way power divider, SIW bend, and SIW waveguide which are discussed later in detail. All the three modules are designed to be operated over a wide frequency range and these modules can be used in constructing a 2^N (N=1, 2…) way

SIW power divider. Also these components can be integrated directly in constructing any power divider geometry [11]. Thus, a 1:8 power divider is constructed using these modules as shown in Figure 3.1.

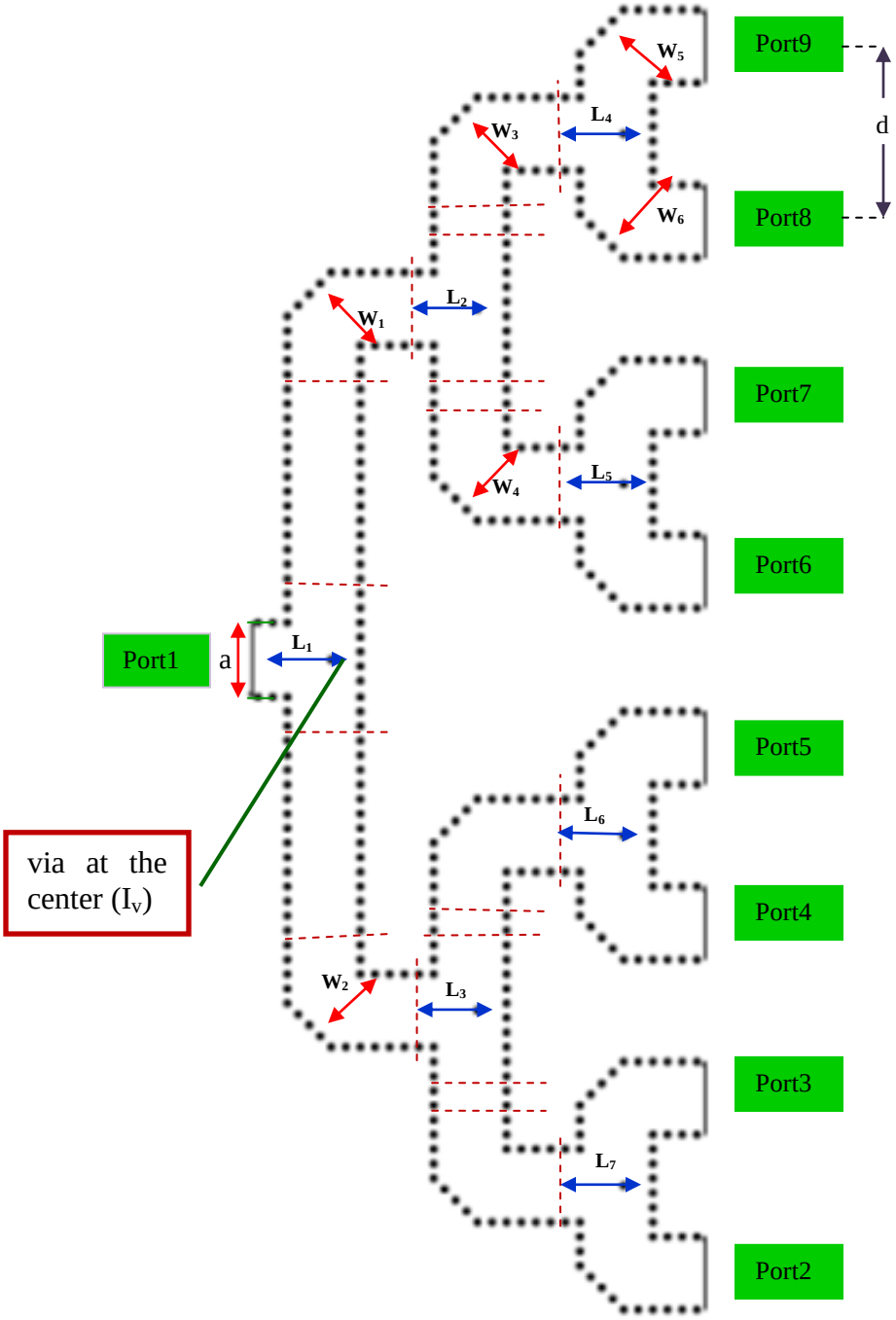

Figure 3.1.Geometry of the 1:8 power divider using hybrid method

The dimensions of the power divider in Figure 3.1 are as follows:

Port width **a** = 7 mm,

radius of the via **r** = 0.3875 mm,

separation between vias (center-center) **s** = 1.37 mm,

$L_1 = L_2 = L_3 = L_4 = 6.83$ mm,

$W_1 = W_2 = W_3 = W_4 = 6.8325$ mm,

distance between the ports **d** = 16.6 mm,

thickness of the substrate **h** = 3.175 mm, and

relative permittivity $\varepsilon_r = 2.2$ with loss tangent 0.002.

The geometry includes seven T-type two way power dividers, and fourteen SIW bends. It can also be observed from Figure 3.1, that each SIW bend is directly integrated with T-type two ways power dividers. The whole structure can be integrated on a single substrate. The modeling of this structure uses a substrate with the relative permittivity (ε_r) of 2.2, loss tangent of 0.002 at 23GHz and thickness of 3.175mm. The rectangular waveguide TE_{10} mode is assumed for all the ports, zero surface impedance is assumed for each metallic via if not otherwise specified, and the port width is chosen to be the width of an equivalent rectangular waveguide [11].

3.2 SIW Fundamental modules:

Before modeling the power divider we have tried to study and examine the building blocks of the feeding network, which are nothing but H-plane SIW T-type 2-way power dividers (T-junction), SIW bends, and a waveguide sections, and based on the distance between the antenna elements (center to center) the number of these blocks can be determined. In order to achieve good performance of the power divider these blocks are designed and optimized. These components can be later used in the study of application of Co-simulation technique to the feeding network.

T-type 2-way power divider (T-junction):

Figure 3.2(a) shows the topology of the H-plane SIW T-type 2-way power divider (T-junction). As indicated in the figure an inductive via (I_v) is placed at the dividing junction, which plays an important role in achieving equal power division.

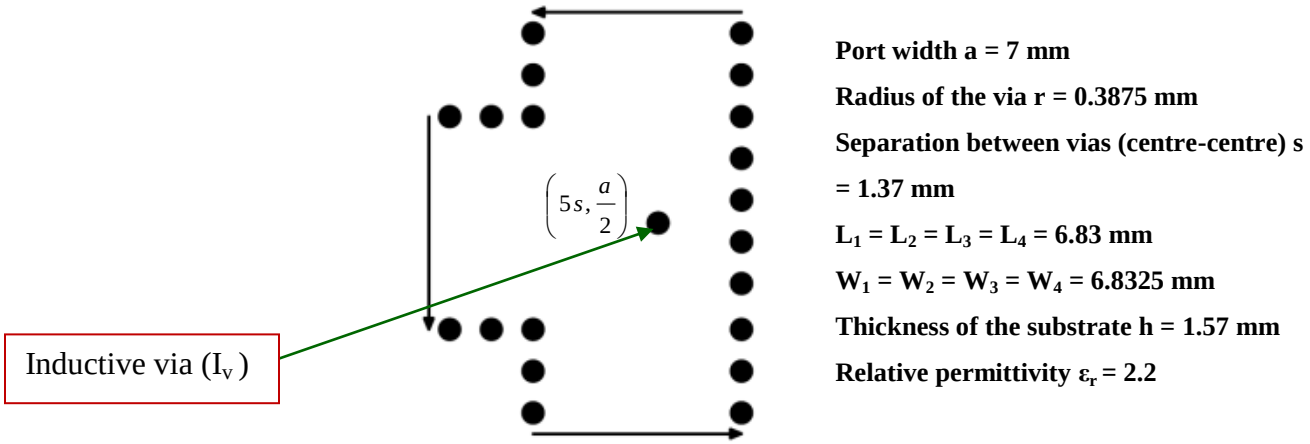

Figure 3.2(a) H-plane SIW T-type two-way power divider (T-junction)

This inductive via (I_v) is placed at a distance of L_1 along the x-axis and at distance of **a/2** along the y-axis from the origin so that it ensures equal power division of the incoming power (from the input port) to the output ports. In general, the inductive via at the center (I_v) is placed nearly $\lambda_g/4$ from the input port (here λ_g is the waveguide wavelength at the operating frequency). The location of the inductive via at the centre (I_v) can be optimized in order to reduce the reflection from the SIW branches, but the initial values for the inductive via can be chosen as $\lambda_g/4$. However, to suppress the higher order modes at the output ports of the SIW T-junction the lengths of each branch of the T-junction are to be chosen longer. Thus by optimizing the position of the inductive via good performance can be achieved for the T-junction power divider. Figure 3.2 (b) shows the S-parameters of an SIW T-type two way power divider.

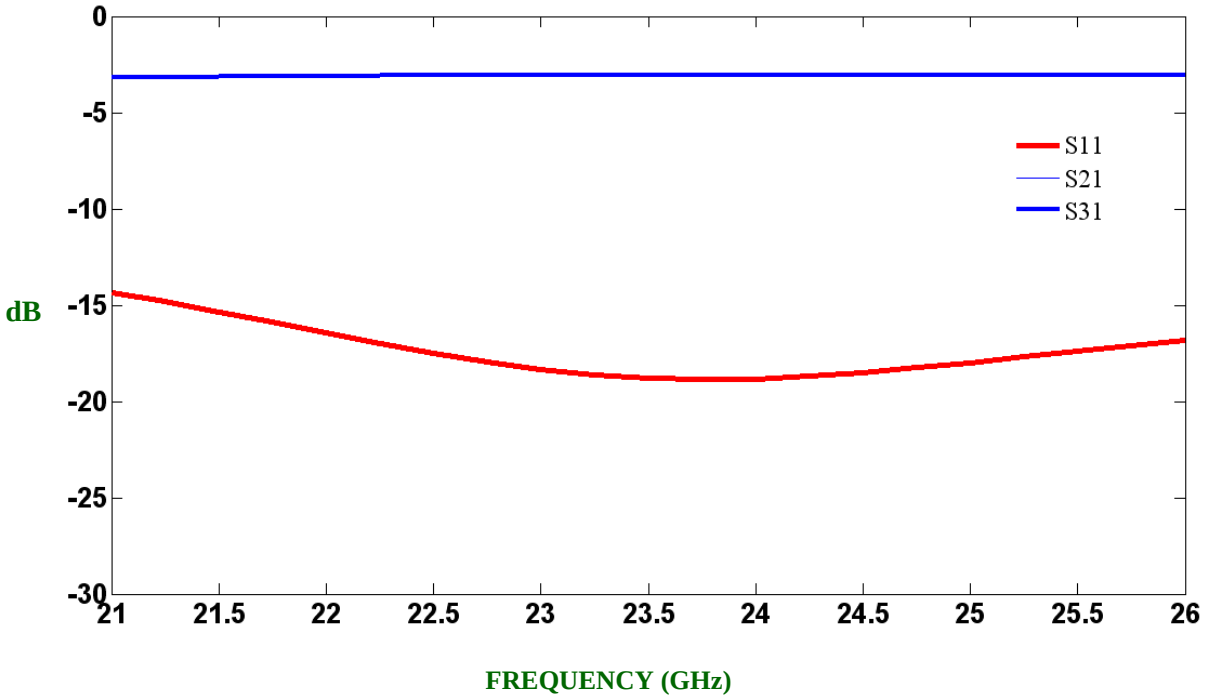

Figure 3.2(b) Reflection co-efficient for the SIW T-type 2 way divider

SIW Bend

The SIW bend shown in Figure 3.3 (a) is one of the fundamental components in the design of a 1:8 power divider (feed network). It can be used in modeling multi-way power divider, and also can be used to change the direction for output ports with an angle of 90 degrees. As indicated in Figure. 3.3(a) the width W_1 is an essential parameter in the performance of the SIW bend and it is the only dimension that can be optimized to obtain low reflection co-efficient for a wideband. Figure 3.3 (b) depicts the S-parameters of the SIW bend. Thus, by optimizing the width W_1, a good performance for the SIW bend can be obtained.

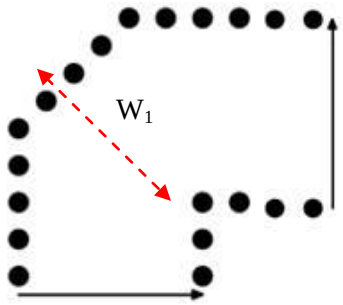

Figure 3.3 (a) SIW bend

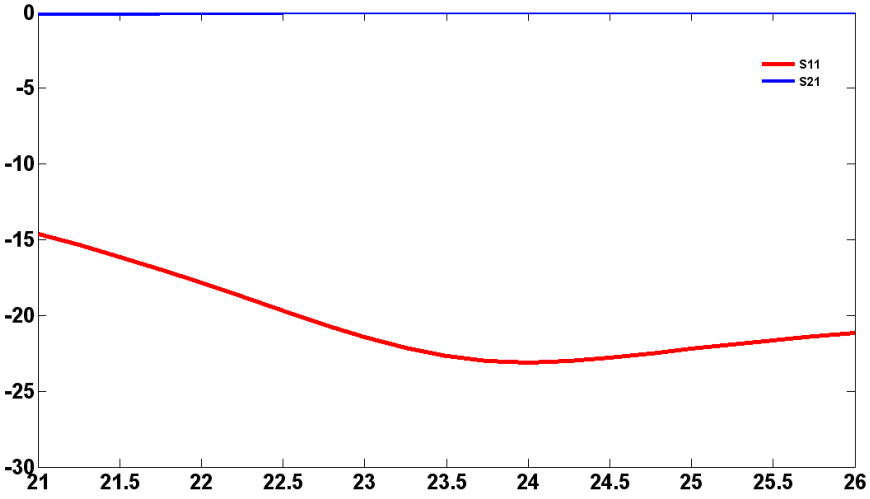

Figure 3.3 (b) Reflection coefficient for the SIW bend

SIW Waveguide

The SIW waveguide is shown in Figure 3.4 (a), which is also one of the fundamental components, in the design of a 1:8 power divider (feed network). This component is used as extensions between the other components (T-junction and SIW bend) in forming the 1:8 power divider. It also plays an essential role of suppressing the higher order modes. The reflection coefficient for the structure is shown in the Figure 3.2 (f)**.**

Figure 3.4 (a) SIW waveguide

However, to cancel the interference between these fundamental modules, the length at the input port can be adjusted. Also to suppress the higher order modes at the output ports of the modules, the lengths of the waveguide sections between SIW T-junction and bend can be increased and if the lengths of these modules` are not long then there is a chance of existence of higher order modes.

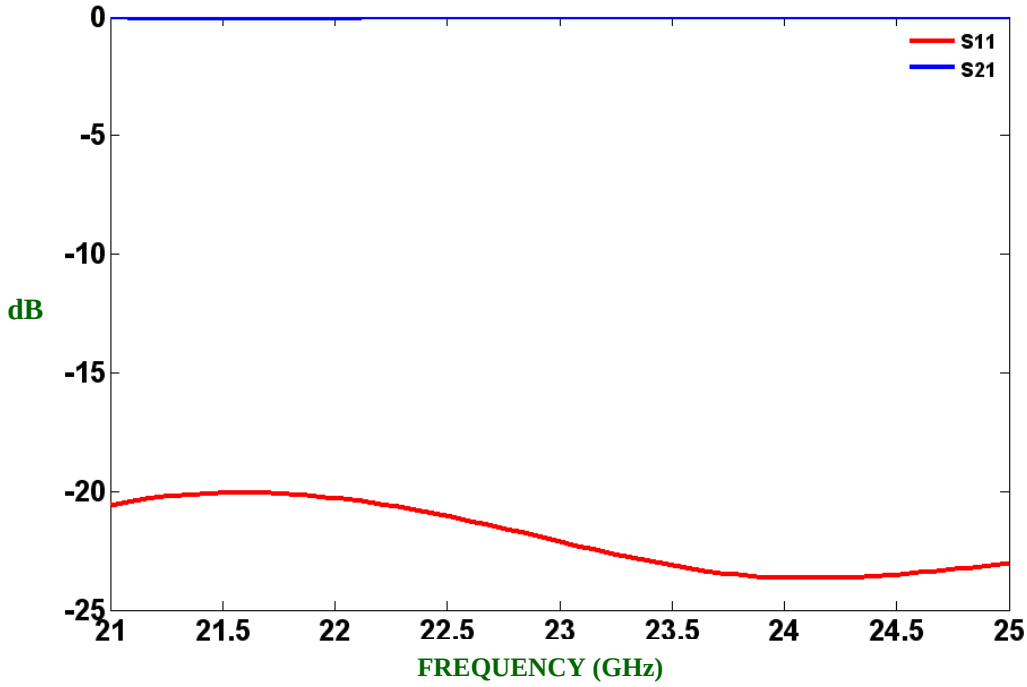

Figure 3.4 (b) Reflection coefficient for the SIW waveguide

It can be concluded that using SIW T-junctions (T-type two way power dividers) and SIW bends a 2^N (N=1, 2…) SIW power divider can be constructed. This method is very convenient to construct a multi-way SIW power divider with equal outputs in magnitude and phases. Here we have tried to compare the s-parameters from the Hybrid method (using C++ code) and from HFSS software (Finite element method). Figure 3.5 shows the feeding network, i.e., the 1:8 power divider, modeled using the simulation software HFSS. In both methods a TE_{10} mode is assumed for all the ports, and zero surface impedance is assumed for each metallic via if not specified. The port width is chosen to be the width of an equivalent rectangular waveguide. Here, for HFSS modeled feed network, initially we have excited each port by the wave port using a partial waveguide, as shown in Figure 3.5, and the vias are designed using regular polyhedrons instead of cylinders for which we can define number of segments.

As the number of segments increases the computation time increases. For more accuracy the number of segments can be further increased. In order to save the computation time we have tried to model the 1:8 power divider by replacing vias with solid walls as shown in Figure 3.6.

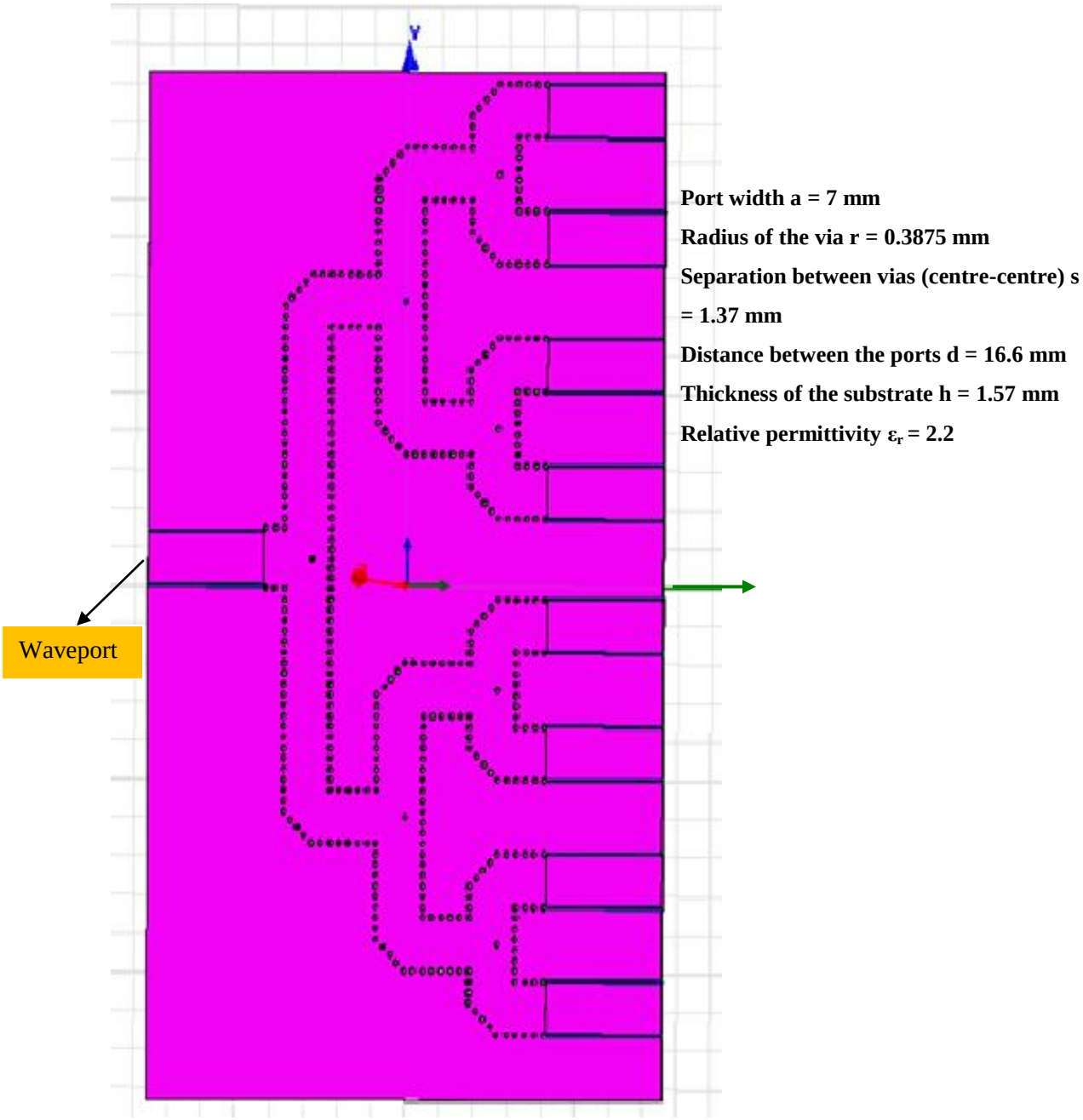

Figure 3.5 1:8 Power divider modeled using HFSS

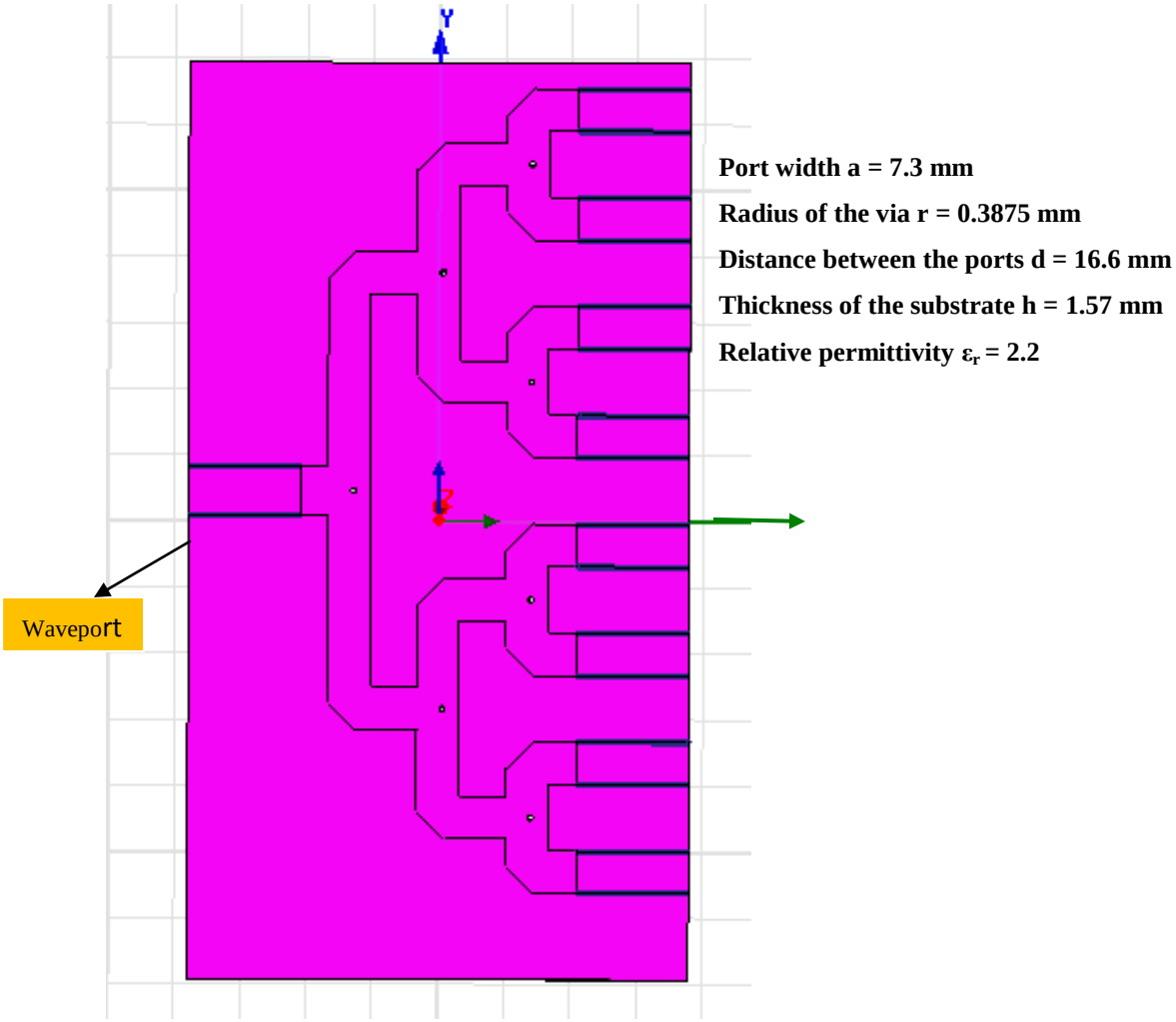

Figure.3.6. 1:8 Power dividers modeled using HFSS replaced by solid walls

In the modeling of the 1:8 power divider using solid walls, the time for the computation is minimum. The main idea behind using metallic solid walls is to minimize the time for optimization, if the geometry of the structure is optimized using solid walls later it can be repeated with metallic vias. This idea makes things simpler in the modeling of the geometries such as power divider, antenna arrays, filters, etc.

An inductive post is used for the equal power division and the modeling of the structure is simple compared to the modeling of 1:8 power divider using vias. Figure 3.7.shows the comparison of the S-parameters for the three cases, i.e., the S-parameters for the 1:8 power divider using the Hybrid Method (C++ code), the 1:8 power divider using HFSS with vias and 1:8 power divider using HFSS with solid walls.

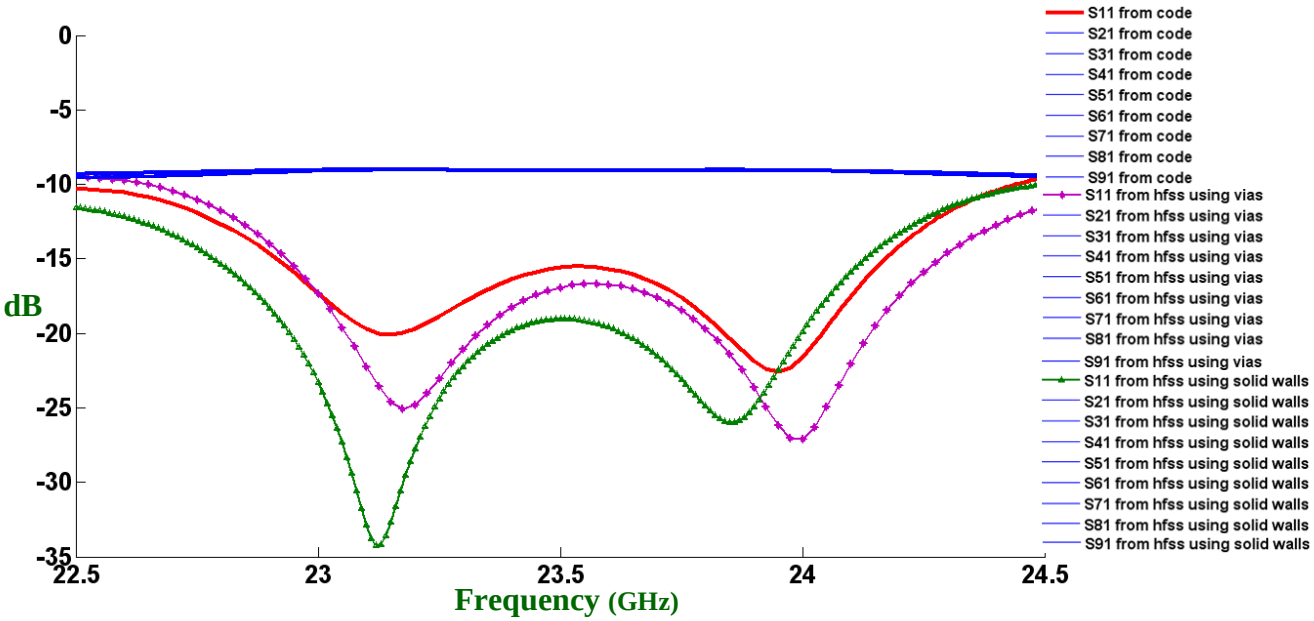

Figure.3.7. Comparison of the s-parameters for all the three cases

It can be observed from the figure that equal power division is obtained in all the three cases. However, S_{11} in the case of the 1:8 power divider with solid walls (using HFSS) is following the S_{11} from the 1:8 power divider using hybrid method (using C++ code). A discontinuity is observed with respect to S_{11} of 1:8 power divider using metallic vias (using HFSS) and this discrepancy can be overcomed by increasing the number of segments for vias. The comparison for the computation time is presented in the Table.3.1.

Table.3.1 Comparison of simulation times

SOFTWARE	MEMORY	TIME(minutes)
CODE	500 GB, 3.5 GB RAM	127
HFSS using metallic vias	500 GB, 3.5 GB RAM	280
HFSS using solid walls	500GB, 3.5 GB RAM	95

3.3 EM CO-SIMULATION TECHNIQUE

In electromagnetics, for the modeling of passive components such as RF filters, multiplexers, couplers, and antennas, three dimensional (3D) simulators such as HFSS, Ansoft designer,…etc., are used, and they provide simulation results that are close to measurement results. However, when the analyzed structure is complex these EM simulation softwares require more computation time for tuning and optimization. In order to overcome this major disadvantage of the EM simulators a technique called EM co-simulation has been proposed [13]. This technique utilizes both the EM- and circuit-based simulators (i.e., EM circuit co-simulation), which provides accurate results with reduced computation times. Figure 3.8 shows the block diagram, which elaborates on the mechanism of EM circuit co-simulation technique [13]. Here, we have tried to apply the co-simulation technique to the feed network which is composed of T-junctions and bends and have tried to validate these results with full wave analysis results.

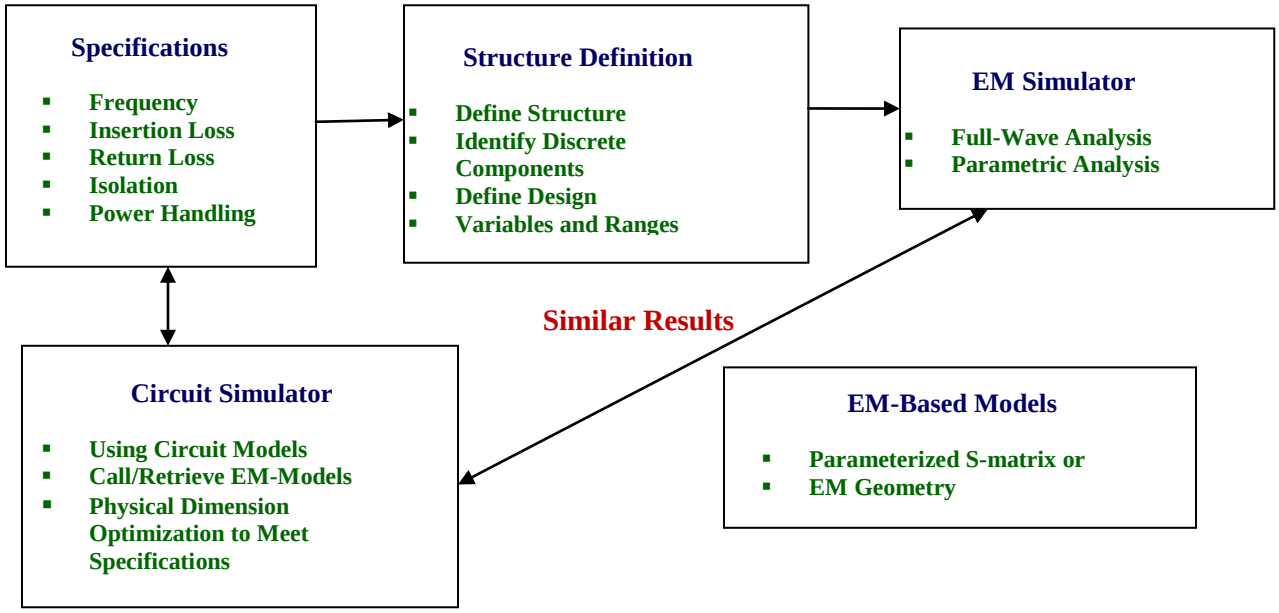

Figure 3.8 EM circuit co-simulation technique

In this method the entire geometry is divided into discrete components (or blocks) as suggested by Figure 3.9. Each component is analyzed individually using an EM simulator. In general, most structures can be separated into a standard set of components such as T-junction, bend, and a waveguide section, as shown in Figure 3.10. Each component's EM analysis is carried out for a range of design variables such as length, width, height, and corner radius [13]. These results are saved as a numerical EM model and could be parameterized. Scattering parameters are imported into a block and used as a component by itself in the circuit simulator which is then used in modeling of the geometry.

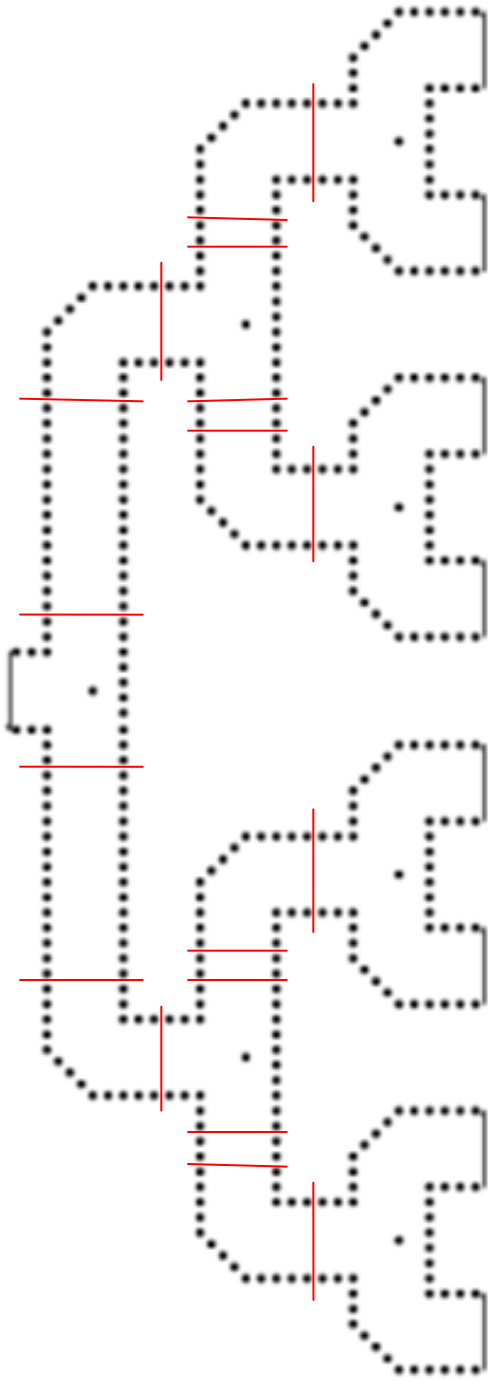

Figure 3.9 Geometry of the 1:8 separated into discrete components

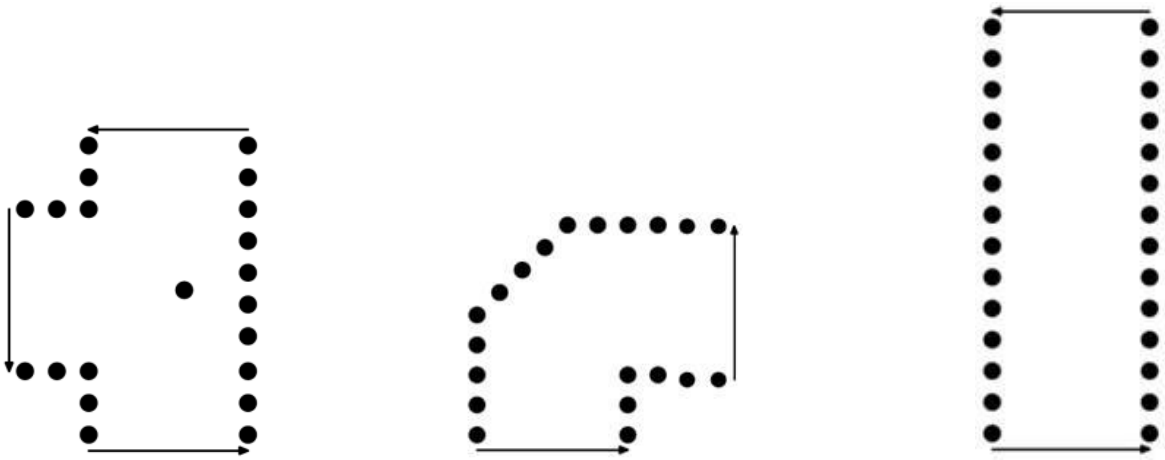

Figure 3.10 (a) discrete components for the 1:8 power divider in EM analysis

Figure 3.10 (b) discrete components for the power divider in circuit analysis (ADS)

A circuit based simulator (here ADS), which is a combination of EM- and circuit –based models is used. In this approach, EM analysis for every combination of dimensions can be avoided during optimization, also faster simulation speed is also achieved. Here, when we applied co-simulation technique to the feed network, which is composed of fundamental components such as T-junction and bend, we have designed each component using the Hybrid method (EM simulator) and optimized them individually, which takes less time when compared with the optimization of the entire structure. The scattering matrices of each component are

imported to circuit simulator component so that a library of circuit simulated components is established in ADS. All the components from the library are assembled together according to the geometry of the power divider and the results are validated with the circuit analysis, which are shown in Figure 3.11.

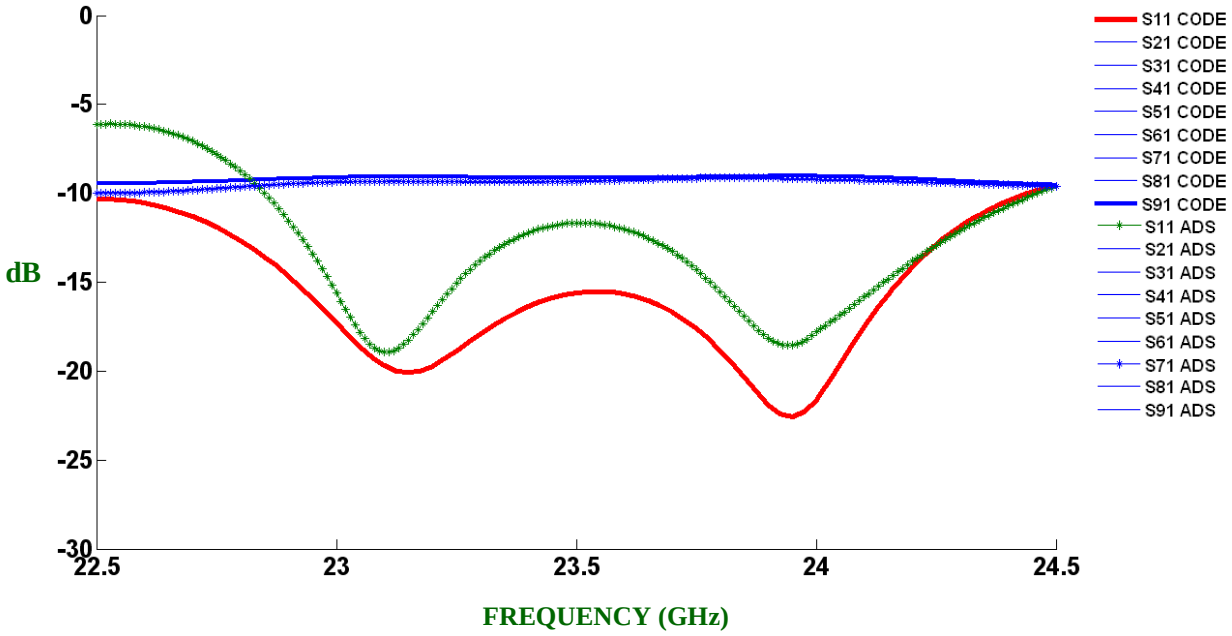

Figure.3.11. Validation of s-parameters using co-simulation technique with the s-parameters from full wave analysis

Thus, full EM simulation of the entire structure is performed just for analysis and not for optimization or tuning. The main advantage of this co-simulation approach is that the EM simulation type accuracy can be obtained with a circuit simulation speed along with optimization.

Table 3.2 Comparison of simulation times

SOFTWARE	MEMORY	TIME(minutes)
ADS	320 GB, 1 GB RAM	1.6
CODE	500 GB, 3.5 GB RAM	127
HFSS	500 GB, 3.5 GB RAM	280

Table 3.2 elaborates the comparison of the simulation time for the 1:8 Power Divider using three different softwares and it can be concluded that among the three softwares, HFSS consumes more time than the other softwares because of the needed fine mesh.

CHAPTER IV

4.1. H-Plane SIW Horn Antenna

The horn antenna is the most widely used microwave antenna. It is used as a feed element for large radio astronomy, satellite tracking, and communication dishes. In addition, it is a common element of phased arrays and serves as a universal standard for calibration and gain measurements of other high-gain antennas. Horn antennas are widely used because of their large gain, simplicity in construction, and preferred overall performance. Horn antennas can take different forms such as the E-plane horn, H-plane horn, Pyramidal horn, conical horn,...etc. The rectangular waveguide horn antennas have found many applications due to their excellent radiation properties such as symmetry patterns, high gain, and very wide bandwidth. But due to the 3D nature and complex size, horns are difficult to integrate with planar circuits and systems. These features limit their use to high performance satellite communications and radar applications [14]. This difficulty is overcome with the SIW technology for H-plane horn antennas, which are easily integrated into planar SIW. This antenna is integrated by using a single substrate, it is easy to fabricate, and the structure is compact. To eliminate the higher order modes in the waveguide the thickness of the substrate is limited [15].

4.11. Design of the Horn

After ensuring the existence of the TE_{10} mode in the waveguide of the SIW horn, the waveguide is flared out in the H-plane to increase the effective radiation aperture, resulting in a narrow beam width in the H-plane [17]. A linear flare in the H-plane only is used in this work and the dimensions of the horn are found following the guidelines provided in [14] to maximize the gain and the dimensions are optimized in order to achieve good performance.

In this work, we have tried to study different cases for the SIW horn and have developed a new modified slot horn antenna. Initially, we have used the thicker substrate of 3.175mm, but later we have ended up using the thinner substrate of 1.57mm. In the beginning of this work, we have used a partial rectangular waveguide for the excitation, which compels the propagation of rectangular waveguide TE_{10} mode through the structure. Later on, when we concluded with the geometry of the horn antenna and feed network, we have used a coaxial cable excitation. With the partial waveguide excitation, we use thicker and thinner substrate, and the TE_{10} mode propagation can be ensured in the structure. For coaxial cable excitation, if the substrate is too thick there is a chance of the existence of the higher order modes. Practically, coaxial cable excitation is used for the measurements, whereas the partial waveguide excitation is not feasible. In order to avoid the higher order modes, thinner substrate is used, but better performance was realized with the thicker substrate as discussed later. A solid wall version is designed later to save full wave simulation time.

Figure 4.1 (a) gives the topology of the SIW horn, which is modeled using HFSS. Initially we have tried to use a partial waveguide that is excited using a wave port, for which a

PEC boundary condition is assigned on the walls of the partial waveguide, and, in a way, we are forcing the TE_{10} mode propagation in the horn. A substrate with the relative permittivity (ε_r) of 2.2, loss tangent of 0.002, and thickness of 3.175mm has been used to model this structure.

Dimensions:

Port width 'a' = 7 mm,
radius of the via 'r' = 0.3875 mm,

separation between vias (centre-centre) 's' = 1.3725 mm,

L_1 = 8.23 mm,

L_2 = 19.14501 mm,
aperture length A = 13.2 mm ($1.51*\lambda_g$),

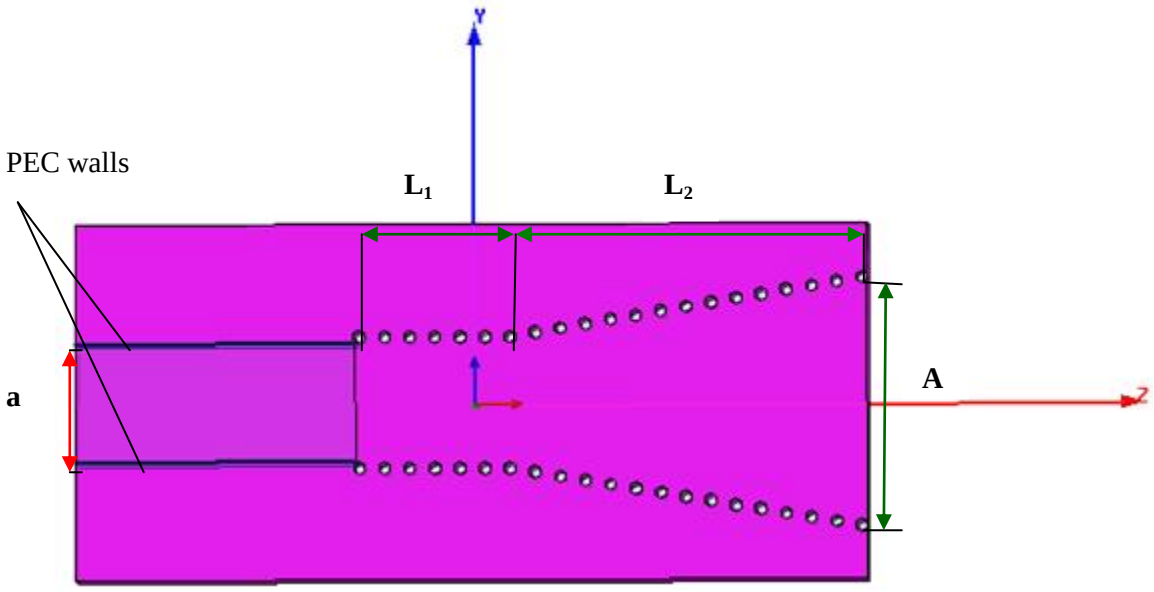

Figure 4.1. (a) Topology of SIW Horn Antenna

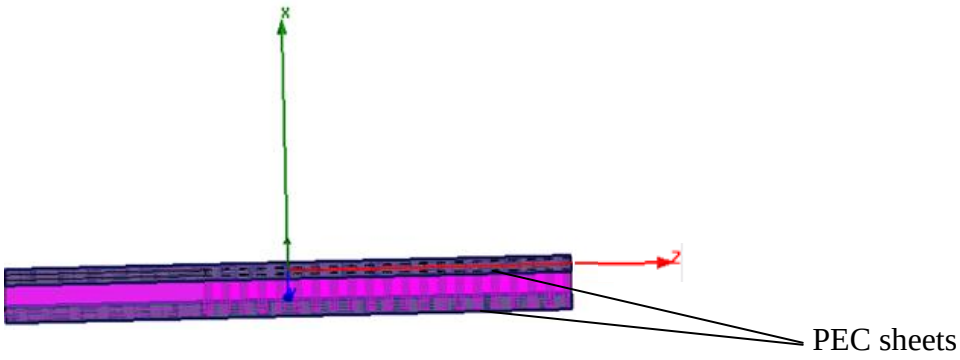

Figure 4.1 (b) H-plane SIW horn antenna another view

From Figure 4.1 (a), it can be observed that two rows of metallic vias are used to form a waveguide long enough to establish the existence of TE_{10} mode alone. The waveguide then flares out in the H-plane resulting in an SIW H-plane horn. These vias are covered by the PEC sheets at the top and bottom in order to make sure that the fields are bounded between these rows of metallic vias. The electric field distribution for this geometry is shown in Figure 4.1 (c), where it can be observed that a single mode is propagating throughout the waveguide. After the flaring, single mode propagation exists, a discontinuity is observed at the aperture. This discontinuity is because of the two reasons, the first reason is due to no substrate immediately after the last via of the geometry, and the second reason is that the conductor sheet ends immediately after the last via of the geometry, because of these reasons most of the power is reflected back. The radiation pattern and reflection coefficient are shown in Figure 4.1 (d), Figure 4.1 (e), and Figure 4.1 (f) respectively.

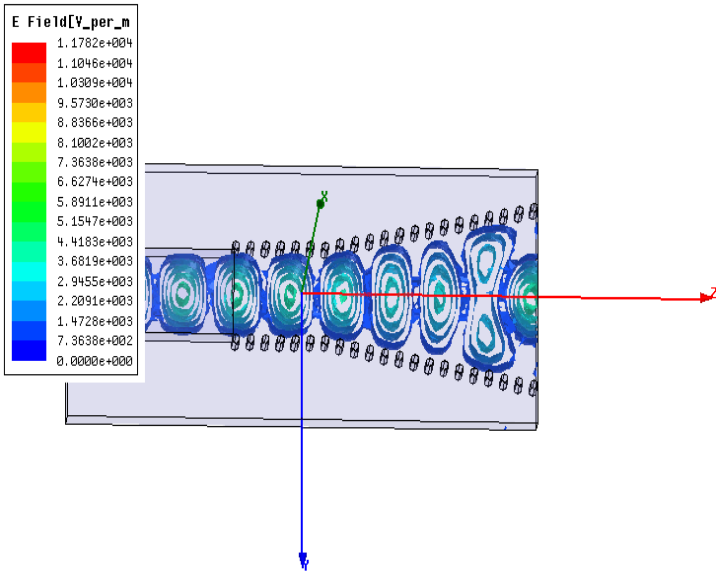

Figure 4.1 (c) Electric field distribution of the H-Plane SIW horn antenna

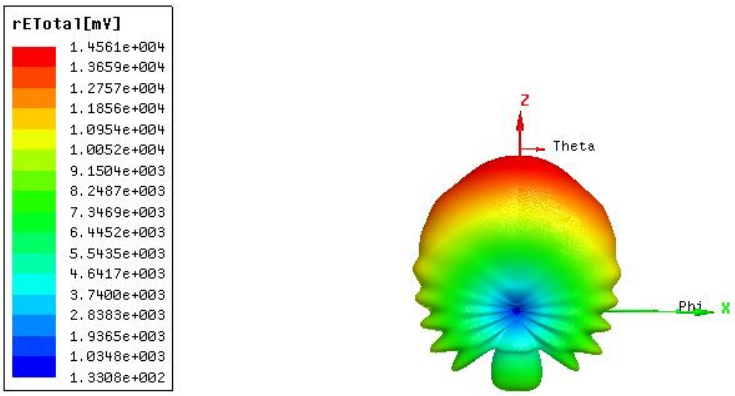

Figure 4.1 (d) 3D Radiation pattern at 23GHz

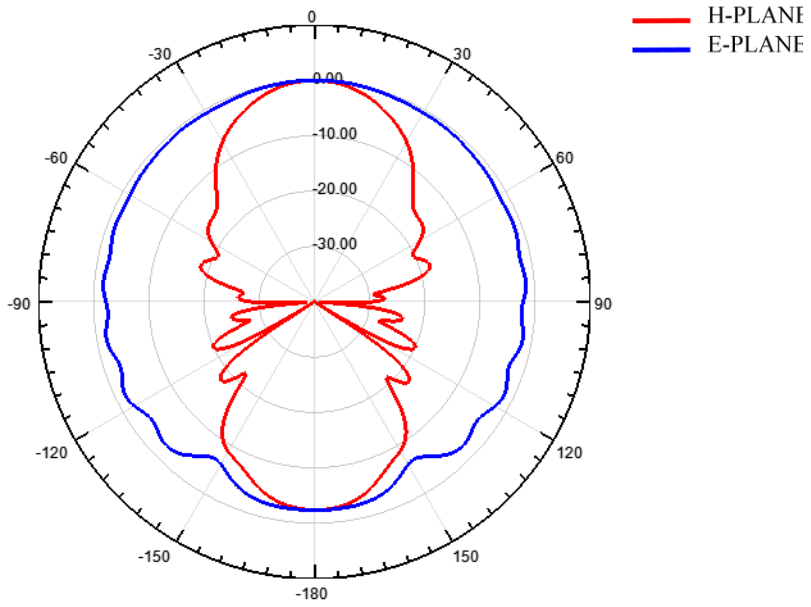

Figure 4.1 (e) Far field radiation patterns of the H-plane SIW horn at 23GHz

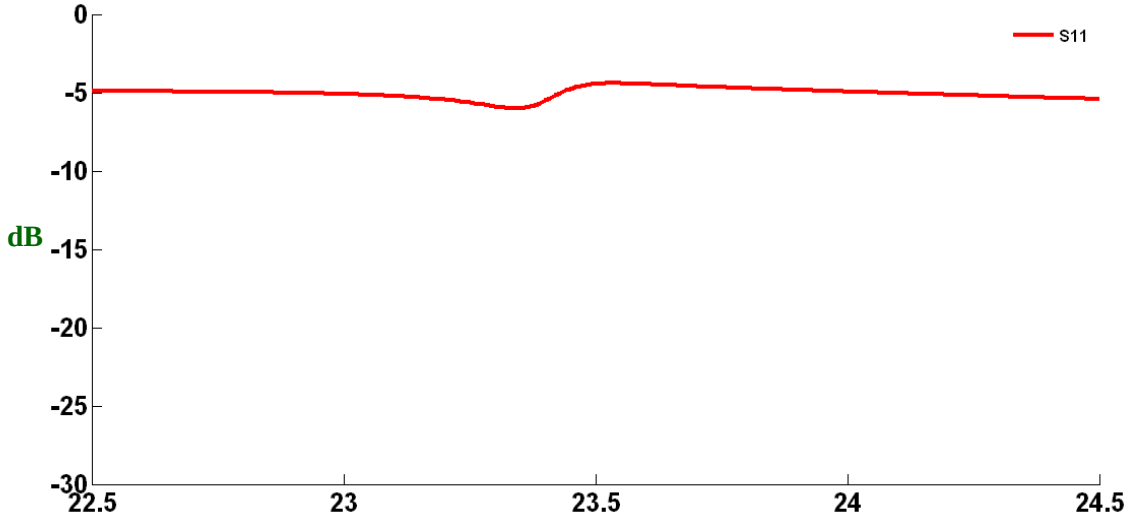

Figure 4.1 (f) Reflection coefficient of the H-plane SIW horn

Due to the discontinuity at the aperture of the horn, it can be observed from Figure 4.1 (f) that the power is reflected back. Thus, in order to overcome the discontinuity we have tried to use the following:

Dielectric Lens

- rectangular Lens
- elliptical lens

Slot

- single slot
- double slot

4.2. SIW Horn Antenna with Dielectric Lens

A Dielectric lens may be used to reduce the beamwidth, increase axial gain and to achieve non-mechanical beam scanning. Also, it can also be integrated in an array easily and can be fabricated easily. In order to overcome the discontinuity, we have tried to place a dielectric load at the opening of the horn. Generally, this loaded dielectric slab in front of the horn aperture is considered as a dielectric guiding structure excited by the horn aperture and it results in a narrower beamwidth in the E-plane, and in the case of H-plane, for a maximum gain horn, the aperture phase distribution along the H-plane is nearly uniform. However, if the length the slab is not properly chosen the beamwidth in the H-plane will be broadened. Thus, by choosing the

proper length of the dielectric lens the beamwidths in the E-plane and H-plane can be narrowed and also high gain can be achieved. The Dielectric load in some cases plays a vital role in improving the reflection coefficient [15]. Figure 4.2 shows the SIW horn antenna with dielectric load. The length of the dielectric load can be optimized until the main beam becomes more directive and the radiation pattern in the E-plane and H-plane are narrowed.

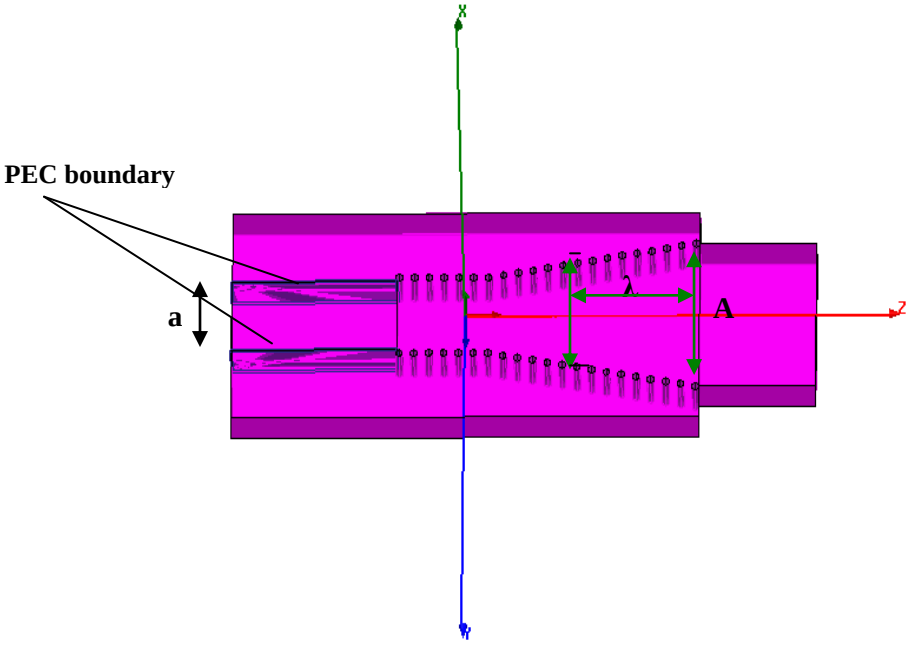

Figure 4.2 Dielectric loaded SIW horn antenna

In this case we started with the length of the dielectric slab as a quarter wavelength and we found that when the length of the dielectric slab is lambda (λ), which is 13.36 mm, the main beam becomes narrow and the radiation pattern in both the E-plane and H-plane is narrowed which can be observed from the Figure 4.3 (a) and Figure 4.3 (b).

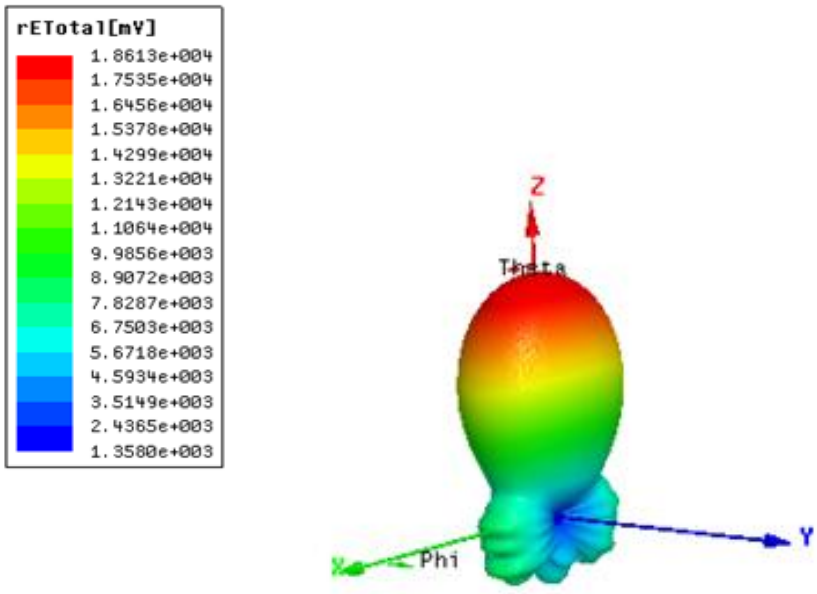

Figure.4.3 (a) Three-Dimensional Radiation Pattern at 23GHz

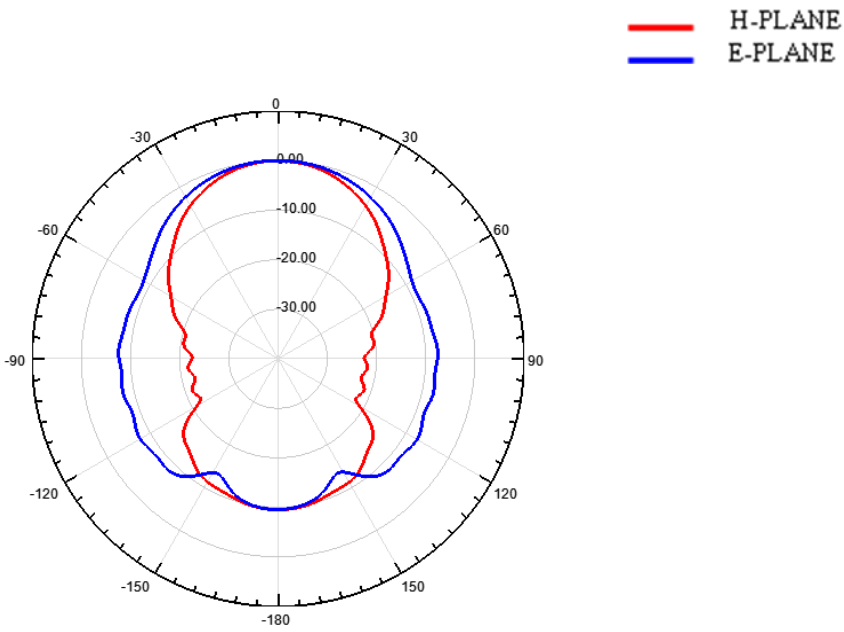

Figure 4.3 (b) far field radiation patterns of the dielectric loaded H-plane SIW horn at 23GHz

The electric field distribution for the dielectric loaded horn is shown in Figure.4.4. Still the problem persists and in order to fix this problem we have tried to make a slot on the copper sheet on the top of the substrate without disturbing the substrate.

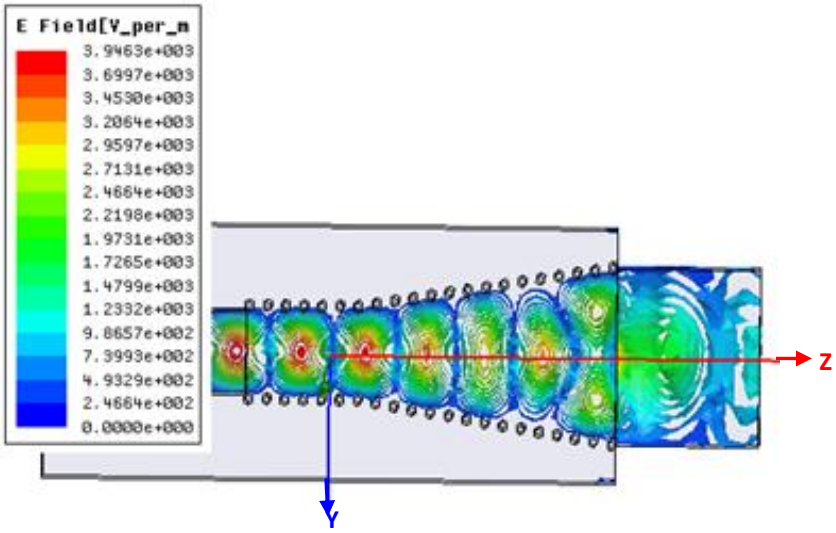

Figure 4.4 Electric field distribution for the dielectric loaded horn

4.3. SIW Horn Antenna with Reflection Cancelling Slot Pair

To fix the discontinuity at the aperture we have tried different things, such as a single slot on one side (upper PEC of the horn) [16], a dielectric load to the SIW horn with a single slot on one side, etc., and then we came up with the horn antenna with reflection cancelling slot pair on upper conducting sheet of the horn without disturbing the substrate, as shown in Figure 4.5. The most essential feature of the reflection canceling slot pair is that the reflections from the two slots are canceling each other since the path length between them is about 180 degrees and the coupling between them is preserved. The main advantages of these reflection canceling slot pairs

is that a wide frequency bandwidth in terms of reflection and gain is obtained due to the traveling wave excitation [18]. The lengths of the two slots, L_3, and L_4, the widths of the two slots, and the separation distance between the slots can be optimized to suppress the reflection from the slot pair. Also, the positioning of the slots plays a critical role for the antenna radiation.

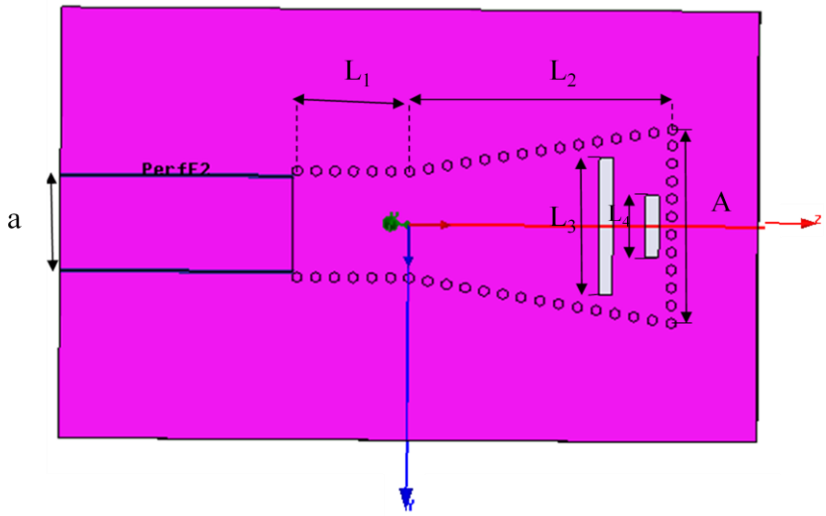

Figure 4.5 Horn antenna with reflection cancelling slot pair

The antenna dimensions are as follows:

Port width 'a' = 7 mm,
radius of the via 'r' = 0.3875 mm,

separation between vias (centre-centre) 's' = 1.37 mm,

L_1 = 8.23 mm, L_2 = 19.145mm,

length of the slot (L_3)= 9.2 mm(λ_g),

length of the slot (L_4)= 3.2 mm,

width of the slot = 1 mm,

aperture length A = 13.2 mm(1.51*λ_g),
thickness of the substrate 'h' = 3.175 mm , and
relative permittivity ε_r = 2.2 with loss tangent of 0.002.

From Figure 4.5 it can be observed that the opening of the horn is closed by a wall of vias to avoid the radiation through the aperture and a pair of rectangular slots is made on the conducting sheet at the top of the substrate near to the aperture without disturbing the substrate, one of them is longer than the other. These slots are separated by a distance of about the quarter guided wave length and both the slots are of the same width of 1mm. Figure 4.6 depicts the electric field distribution of the antenna. Single mode propagation is observed throughout the antenna radiating through these slots. It is radiating in such a way that, if first slot is radiating then the second one is gathering the remaining power with which it is radiating again. At the same time the reflections from the two slots are canceling each other. Thus, we can conclude that it is not a horn anymore and is just a slot antenna as the entire structure is radiating through these slots. The 3-dimensional radiation pattern of the antenna is shown in Figure 4.7.

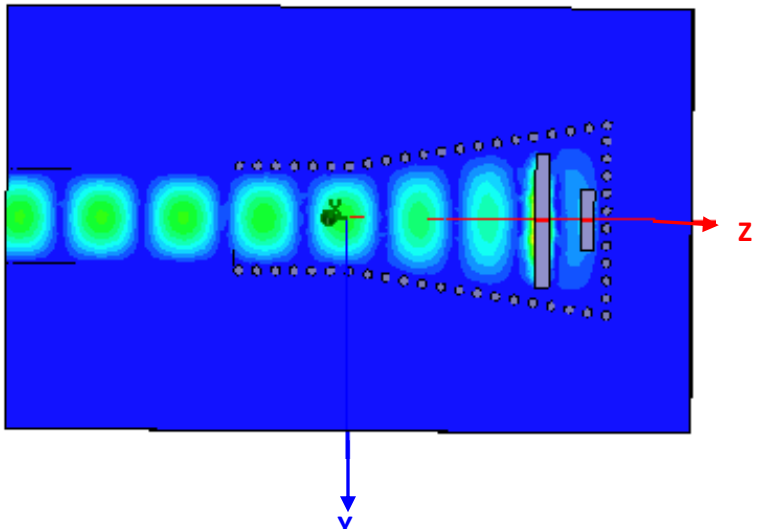

Figure 4.6 Electric field distribution for the horn antenna with reflection cancelling slot pair

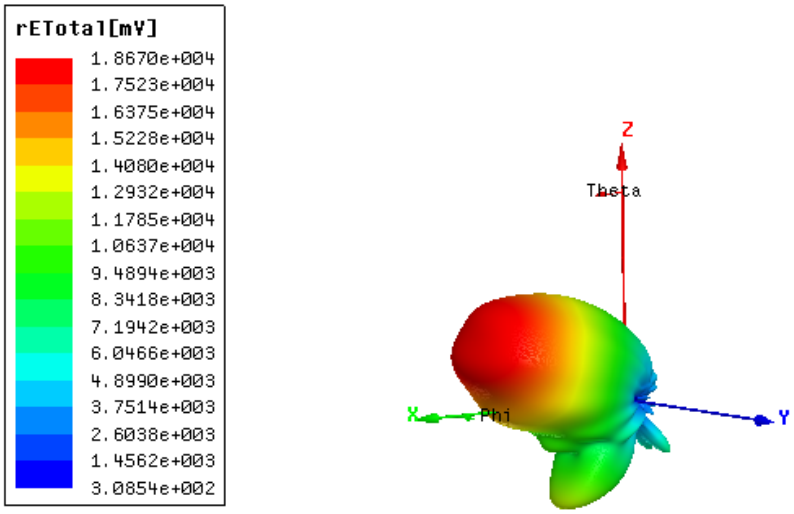

Figure 4.7 Three dimensional radiation pattern at 23GHz

From Figure.4.7, it can be observed that the main beam is tilted towards the X-axis (even though it is narrow) this is due to the reason that the aperture is closed and slots being on upper conducting sheet (one side) of the horn in XZ plane, because the antenna is propagating in that particular plane, but the goal was to make antenna radiate along the Z-axis in the direction of the aperture.

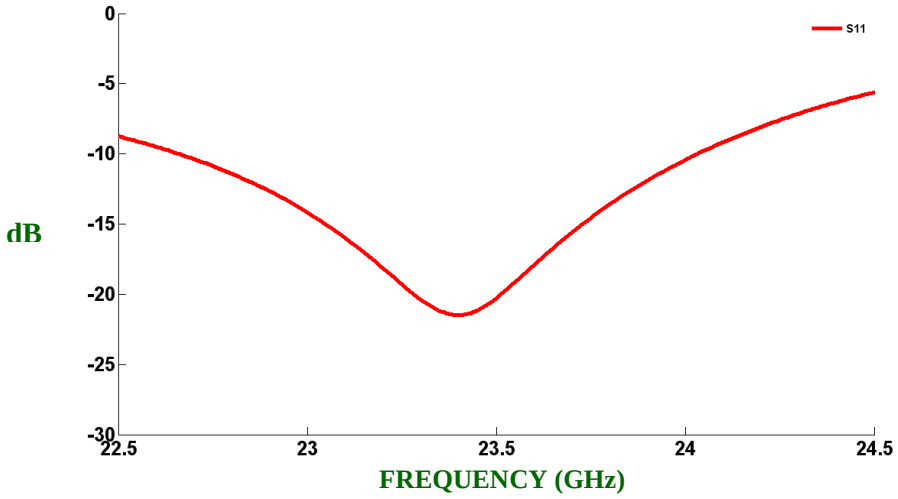

Figure 4.8 Reflection coefficient for Slot Antenna

Figure 4.8 depicts the reflection coefficient for the slot antenna. Matching is improved in this case compared to the other cases, and a reflection coefficient of less than -15dB is achieved from 23GHz to 24GHz.

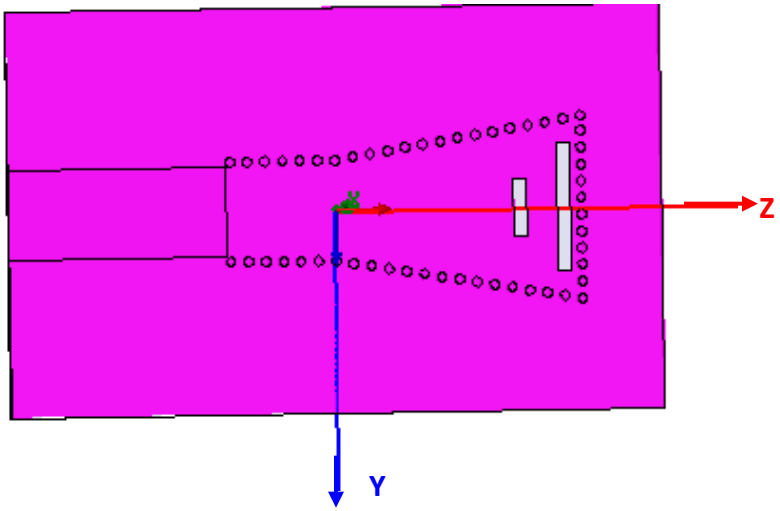

Figure.4.9 Slot Antenna with the slot pair reversed

Similarly, there can be another situation where the position of the slots can be changed, with the smaller slot first and the longer one later as shown in Figure 4.9. For this situation it has been observed that the antenna is radiating in the XY plane with a high reflection coefficient. Thus, we have concluded with the horn antenna with reflection canceling slot pair, longer slot followed by the shorter slot on upper conducting sheet.

4.4. Modified horn slot antenna

It has been seen in the previous section that if we have a slot pair on one side of the horn, it is radiating in that particular plane. Thus we have tried to make slot on both upper conducting sheet and the lower conducting sheet without disturbing the substrate so that antenna can radiate in direction of the aperture.

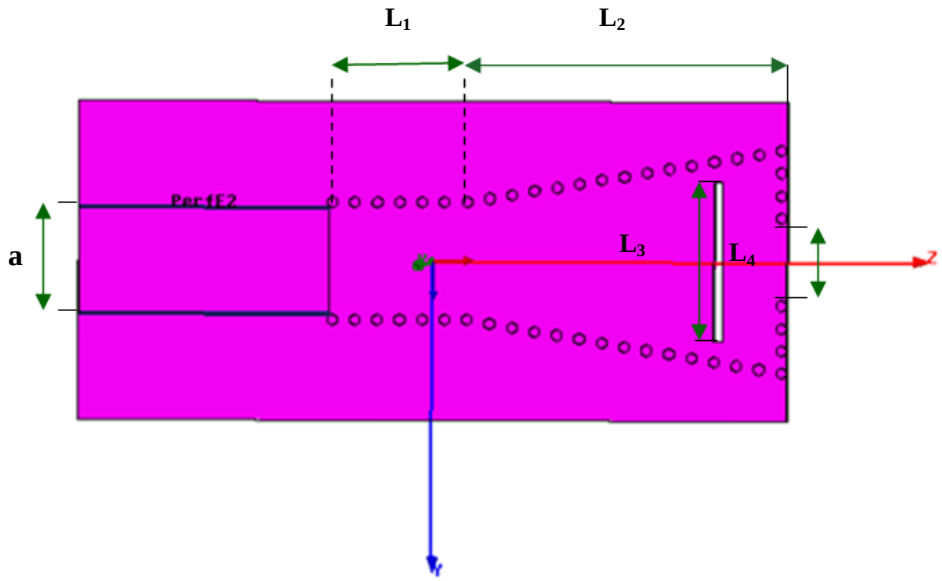

Figure 4.10 Modified horn slot antenna

Dimensions for the antenna shown in Figure 4.10 are as follows:

Port width '**a**' = 7 mm,

radius of the via '**r**' = 0.3875 mm,

separation between vias (centre-centre) '**s**' = 1.37 mm,

L_1 = 8.23 mm & L_2 = 19.145mm,

length of the slot (L_3)= 10.858 mm($1.1*\lambda_g$),

length of the slot (L_4)= 5.1796 mm($0.56*\lambda_g$) and spacing between the slots is 3.918 mm,

width of the slot = 0.6 mm,

aperture length **A** = 13.2 mm($1.51*\lambda_g$), and

thickness of the substrate '**h**' = 3.175 mm

relative permittivity ε_r = 2.2 with loss tangent of 0.002.

When we closed the aperture with the wall formed by the metallic vias, the antenna was radiating through the slot pair and was acting as a slot antenna. In order to avoid this we have tried to make an opening at the aperture by removing a few vias. This opening act as a common opening to both the upper and lower conducting sheets. Also, it acts as a small slot and similar radiation mechanism of reflection canceling pair can be observed. The electric field distribution for the modified horn slot antenna is shown in the Figure 4.11. Antenna is radiating through the longer slot initially, and then the remaining power is accumulated by the smaller slot with which it is trying to radiate again. At the same time the reflections from the two slots are canceling each other. Thus, it is no more a slot antenna as it is radiating through the small aperture and we have concluded it as modified horn slot antenna.

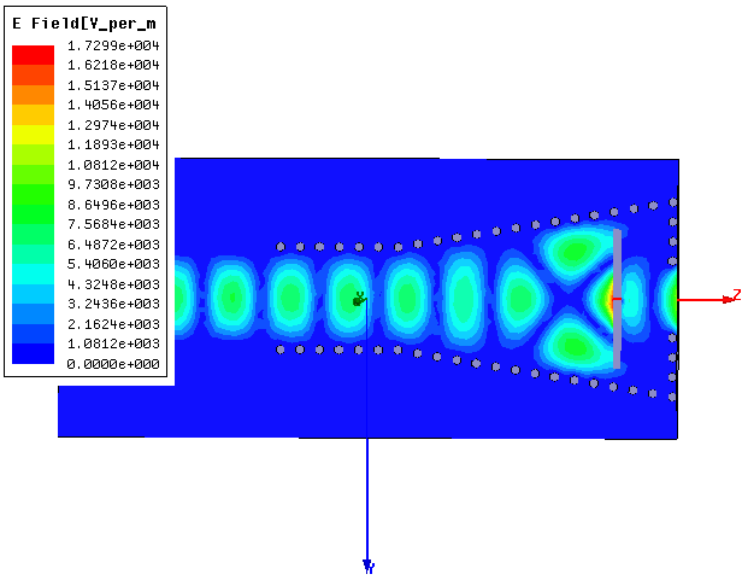

Figure.4.11 Electric field distribution of the Modified Horn Slot Antenna

The lengths of the slots, L_3, and L_4, the widths of the slots, the spacing between the slots, and the location of the longer slots can be optimized in order to achieve good performance for the antenna. Also, the length of the small aperture plays a vital role in achieving the resonance for reflection coefficient. The 3-dimensional radiation pattern, radiation patterns in the both E-plane and H-planes for the modified horn slot antenna are shown in the Figure 4.12 (a) and 4.12 (b), respectively.

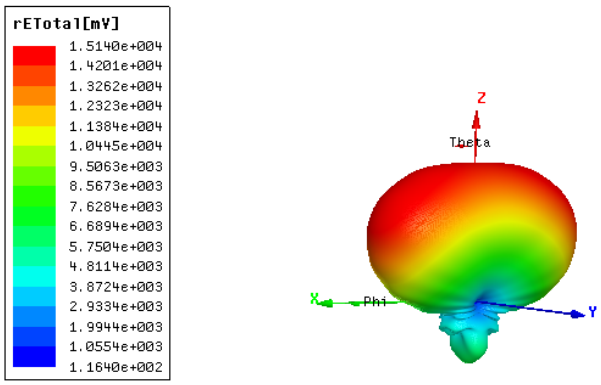

Figure.4.12 (a) 3- dimensional radiation pattern at 23GHz

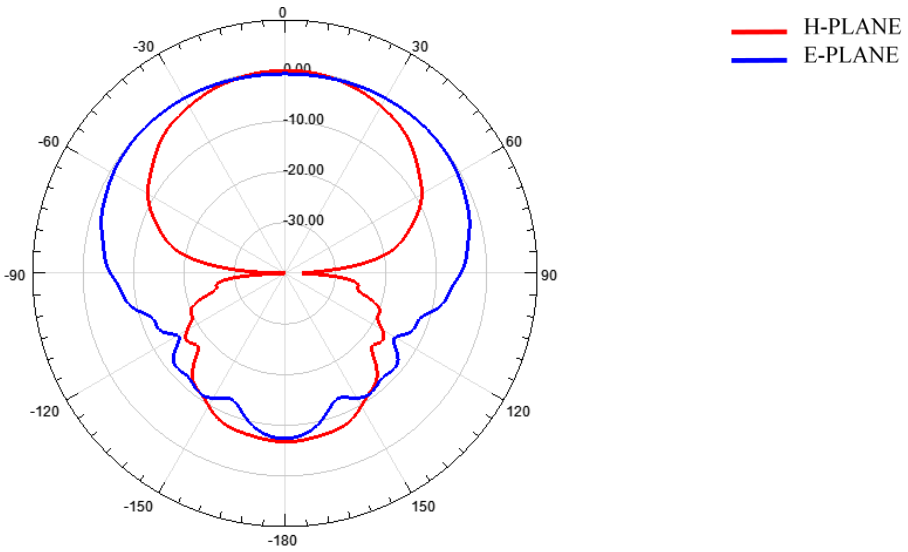

Figure 4.12 (b) radiation patterns in both E-plane and H-plane of the modified horn slot antenna at 23GHz

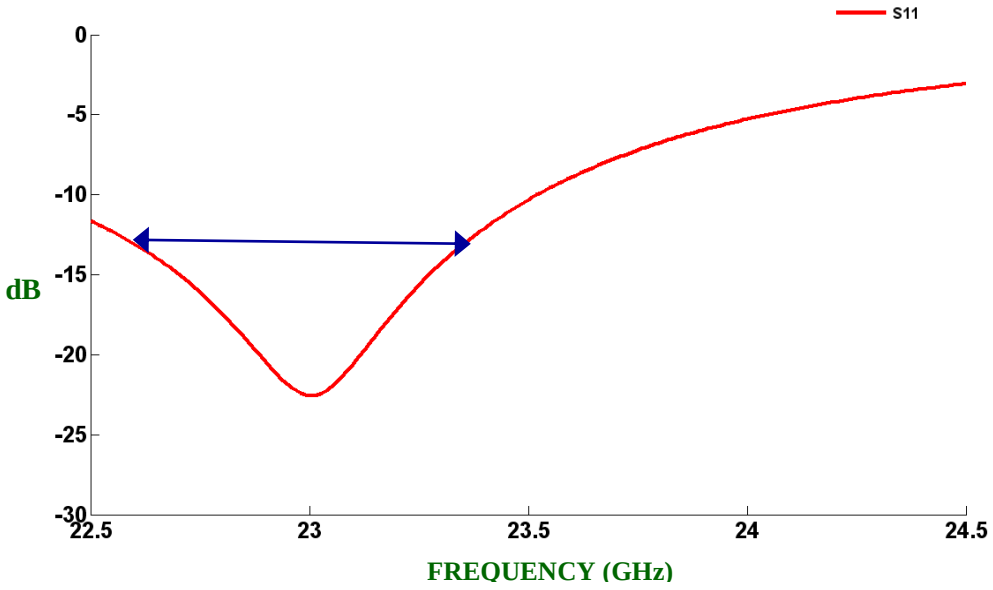

Figure 4.13 Reflection coefficient of the modified horn slot antenna

A broadside radiation is observed for the modified horn slot antenna where the main beam is along the z-axis as shown in Figure 4.12(a), E-plane and H-plane cuts are shown in the Figure 4.12(b). The reflection coefficient of the antenna is shown in Figure 4.13.

4.5. Modified horn slot antenna with dielectric lens

The radiation characteristics of the single element are wide. But, in many applications it is necessary to design antennas with very directive characteristics (very high gains) to meet the demands of long distance communications. However, to obtain a narrow beam we have tried increased length of the horn, and reduced the flaring angle without disturbing the aperture length (A). A dielectric lens is added at the aperture as shown in Figure 4.14.

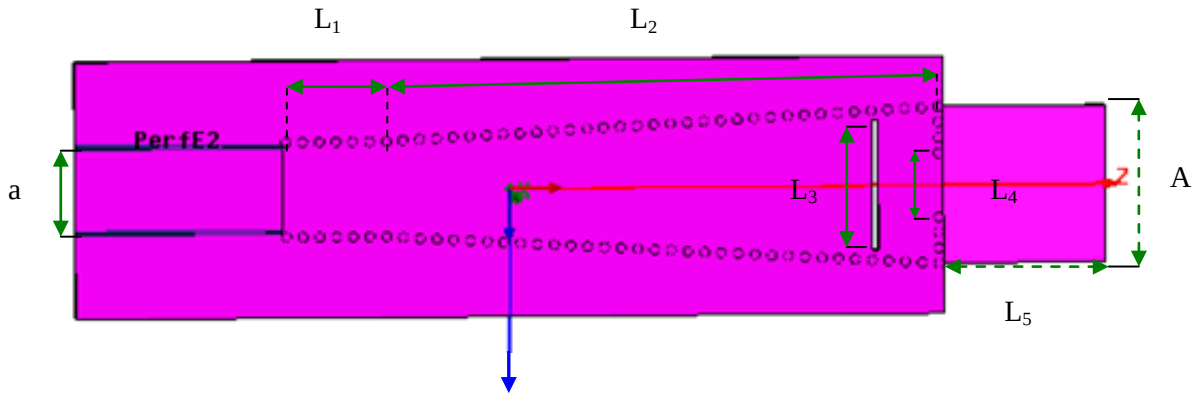

Figure 4.14 Modified horn slot antenna with dielectric lens

The dimensions of the antenna in Figure 4.14 are as follows:

Port width ‘a’ = 7mm,

radius of the via ‘r’ = 0.3875 mm,

separation between vias (center-center) ‘s’ = 1.37 mm,

L_1 = 9.607 mm & L_2 = 43.919 mm,length of the slot (L_3)= 10.62 mm($1.1*\lambda_g$),

length of the small aperture (L_4)= 5.23 mm($0.56*\lambda_g$) and spacing between the slots is 3.918 mm,

width of the slot = 0.5 mm,

length of the lens = 13.32 mm,

aperture length = 12.8 mm,

flaring angle $\alpha = 3.179^0$,

thickness of the substrate ‘h’ = 3.175 mm, and

relative permittivity ε_r = 2.2 with loss tangent of 0.002.

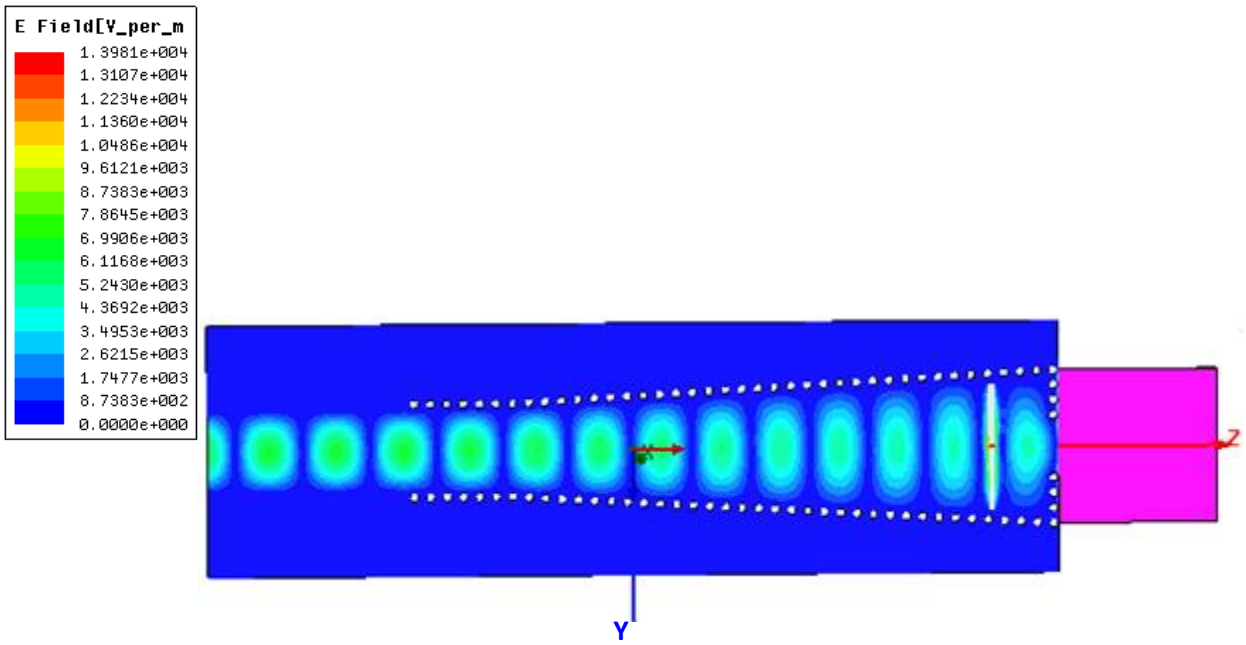

Figure 4.15 Electric field distribution of the dielectric loaded modified horn slot antenna

Figure 4.15 depicts the electric field distribution for the antenna. Because of the decreased flaring angle and increased length of the horn, single mode propagation is preserved throughout the structure unlike the previous case.

Due to the lens at the aperture, the main beam is narrowed, which is observed from the 3-dimensional radiation pattern shown in Figure 4.16 (a) and the reflection cancelling slot pair mechanism is preserved due to the presence of the two slots. Figure.4.16 (b) shows that the antenna radiation is narrowed in both E-plane and H-plane.

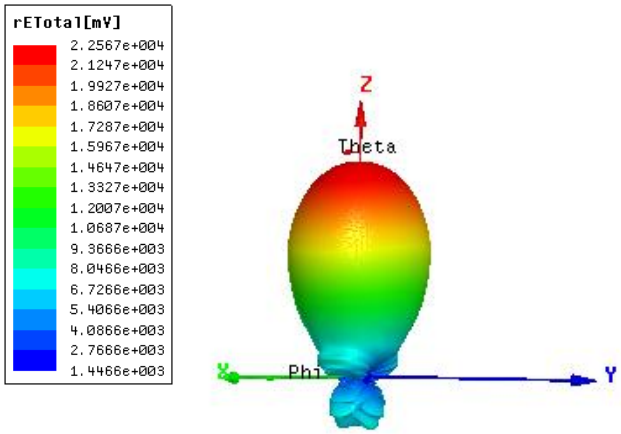

Figure 4.16 (a) 3-dimensional radiation pattern of the dielectric loaded modified horn slot antenna at 23GHz

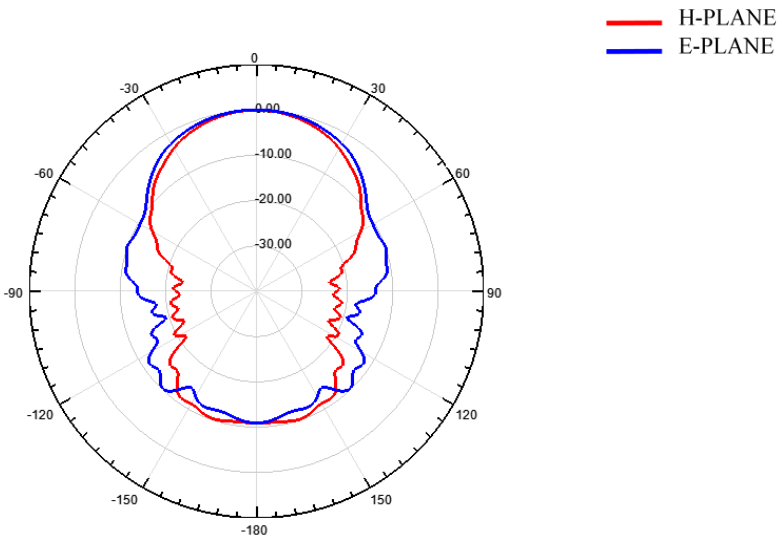

Figure 4.16 (b) radiation patterns in the both E-plane and H-plane of the dielectric loaded modified horn slot antenna at 23GHz

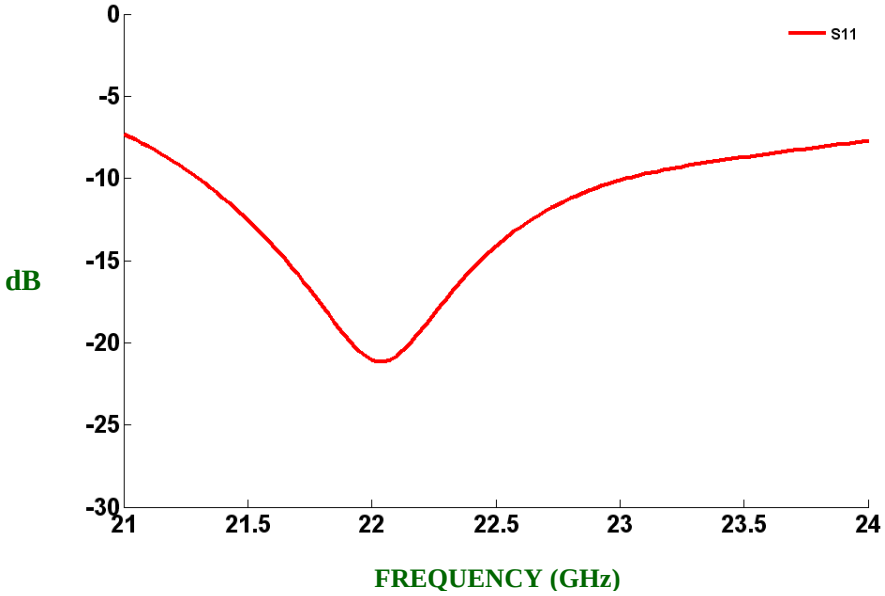

Figure 4.17 Reflection coefficient of the dielectric loaded modified horn slot antenna

The reflection coefficient for the modified horn slot antenna with dielectric lens is shown in Figure 4.17, where one sees that a good matching is obtained. Thus, a horn antenna with the narrow radiation pattern and good matching is obtained. To reduce the computation time for the finite element solution we have tried to replace the metallic vias with the metallic solid walls.

4.6. Modified horn slot antenna with dielectric lens using solid wall

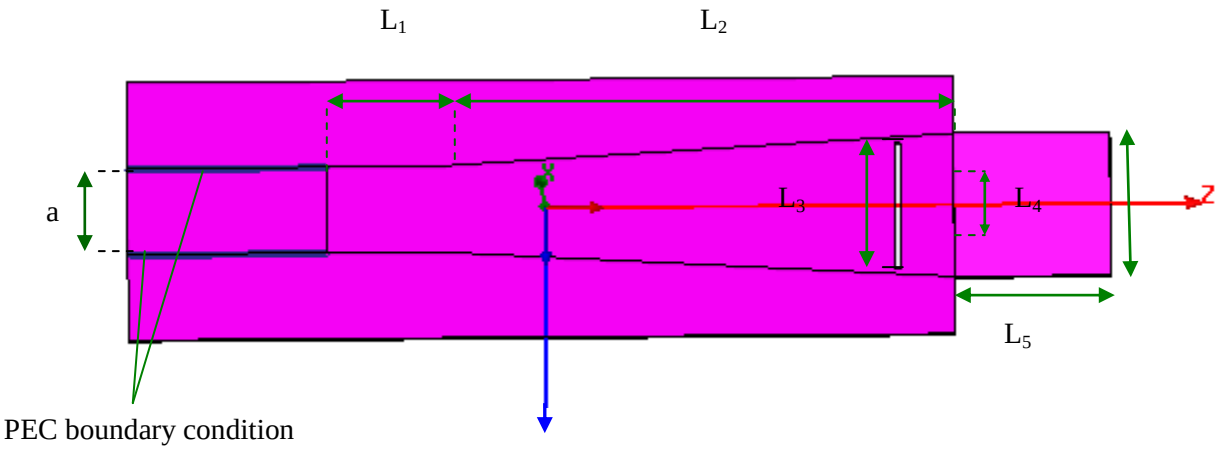

Figure 4.18 Geometry of the Solid wall Horn

Dimensions of the antenna in Figure 4.18 are as follow:

Port width ‘a’ = 7.3 mm,

radius of the via ‘r’ = 0.3875 mm,

separation between vias (centre-centre) ‘s’ = 1.37 mm,

L_1 = 9.607 mm,

L_2 = 43.919 mm,

length of the slot (L_3)= 10.62 mm($1.1*\lambda_g$),

length of the small aperture (L_4)= 5.23 mm($0.56*\lambda_g$),

spacing between the slots = 3.918 mm,

width of the slot = 0.5 mm,

length of the lens = 13.32 mm & height of the lens = 12.8 mm,

flaring angle $\alpha = 3.179^{0}$,

thickness of the substrate 'h' = 3.175 mm,

and relative permittivity $\varepsilon_r = 2.2$ with loss tangent of 0.002.

The geometry of the modified horn slot antenna with dielectric lens using solid walls is shown in Figure 4.18, designed using the SIW equivalence. The electric field distribution in the waveguide and horn for this geometry is shown in Figure 4.19, the comparison for the radiation pattern of the modified horn slot antenna with lens using metallic vias and metallic walls are shown in Figure 4.20.

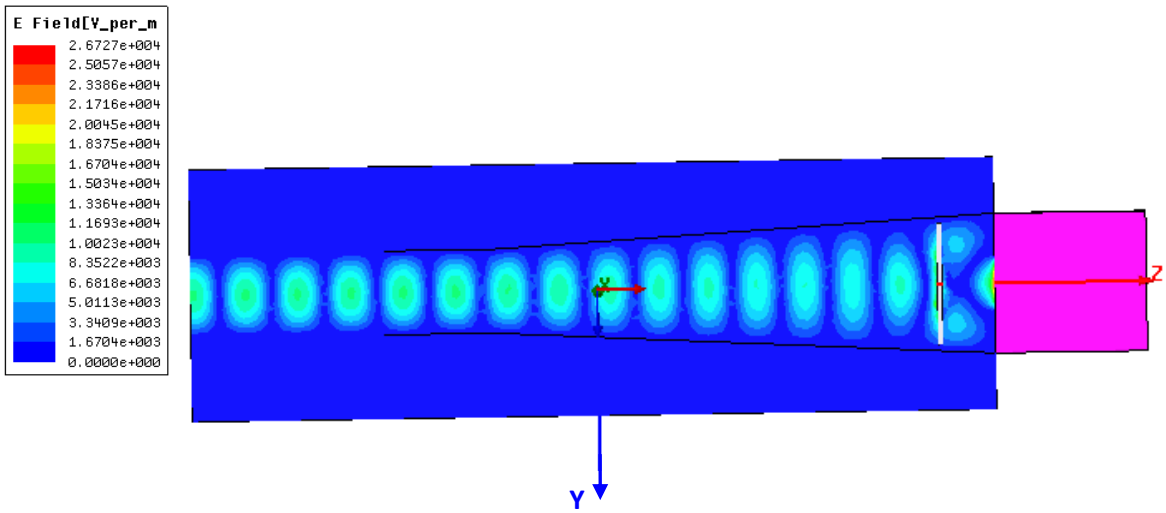

Figure 4.19 Electric field distribution of the solid wall horn

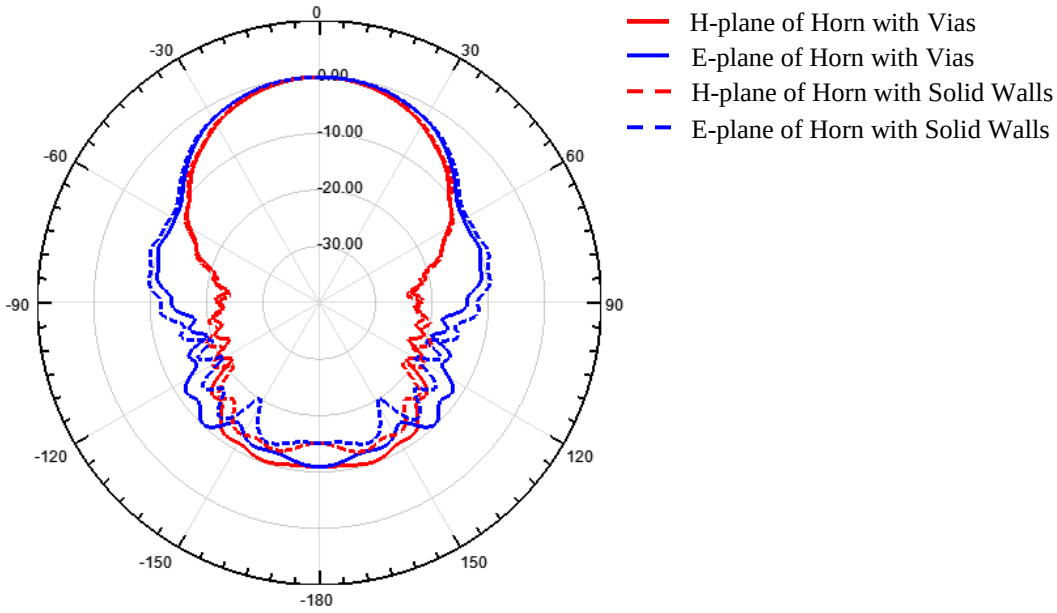

Figure 4.20 far field radiation patterns in both planes for horn antenna with metallic vias and horn antenna with solid walls at 23GHz

The radiation pattern plots shows that the horn antenna with the metallic vias and the horn antenna with the solid walls are similar. It can also be observed there is no leakage in the case of vias. Modeling of the microwave components is simpler using solid walls than using SIW equivalence and reduces the computation time for simulation.

Table 4.1 Comparison of simulation time for the horn antenna

HFSS	MEMORY	TIME (minutes)
Horn Antenna using metallic vias	500 GB, 3.5 GB RAM	198
Horn Antenna using solid walls	500 GB, 3.5 GB RAM	47

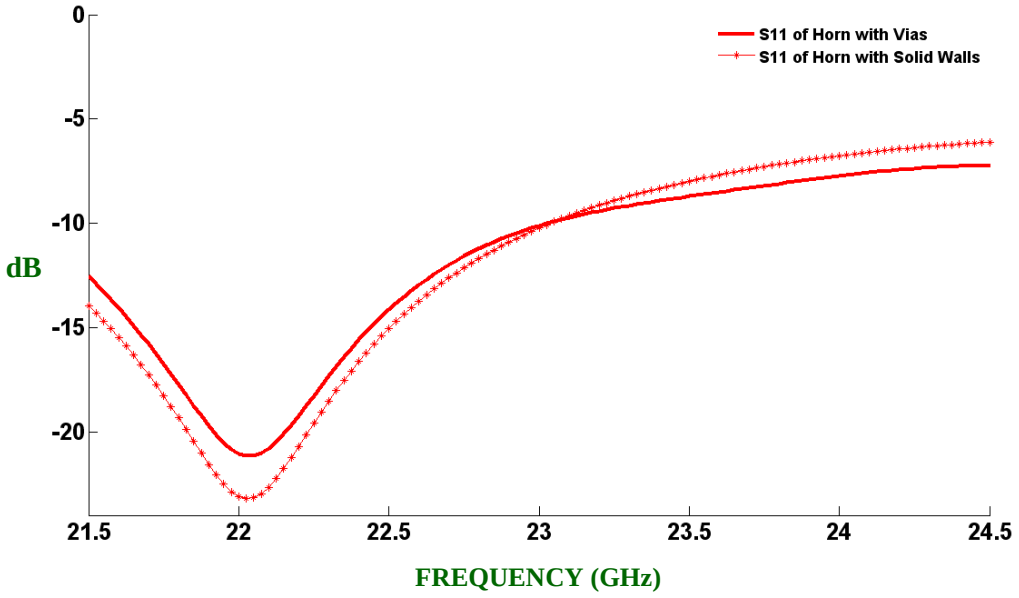

Figure 4.21 Comparison of reflection coefficient for both the cases

The comparison for reflection coefficient for both the cases is shown in Figure 4.21, It can be observed that both are in agreement, but the reflection coefficient for the solid wall horn is lower. Comparison of simulation time for both the cases is shown in Table 4.1

4.7. Modified horn slot Antenna with dielectric lens fed by coaxial cable

Since, the geometry for the antenna element has been determined and the partial rectangular waveguide excitation cannot be used practically, we have tried to excite the horn with coaxial cable. In order to excite the modified horn slot antenna with dielectric lens, a 50Ω coaxial cable is used. Also, the opening of the waveguide is closed with the metallic vias. The dimensions such as the widths of the slots and the height of the probe can be optimized to achieve good matching for the antenna element. The probe is not touching the surface of the substrate. The height of the probe greatly affects the performance of the antenna element. The geometry of the horn antenna using coaxial cable excitation is shown in Figure 4.22 (a).

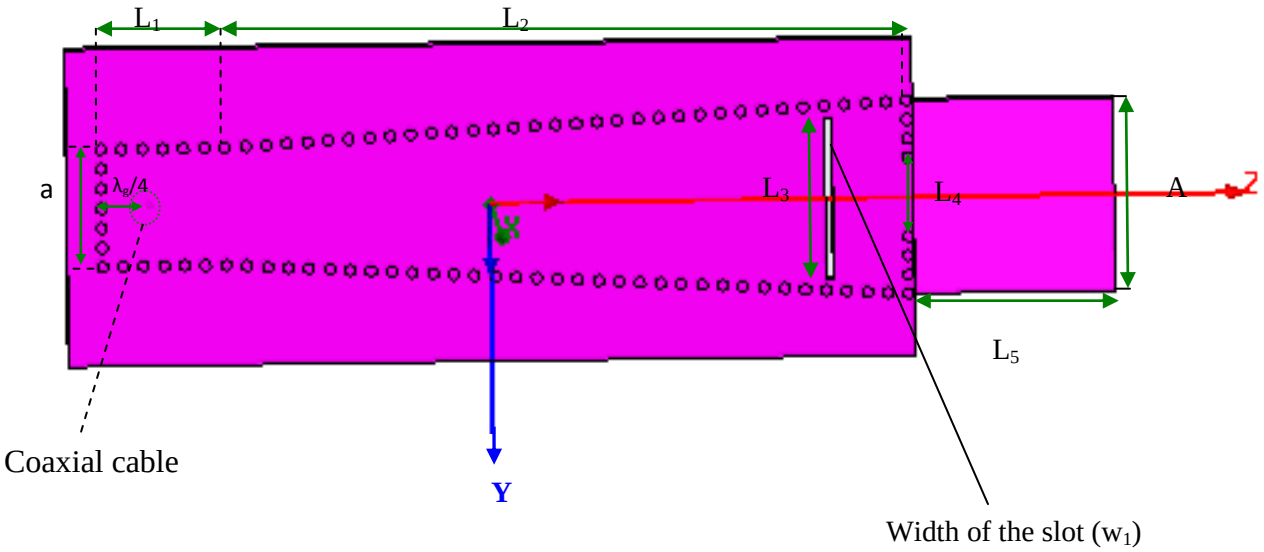

Figure 4.22 (a) Modified horn slot antenna with lens fed by coaxial cable

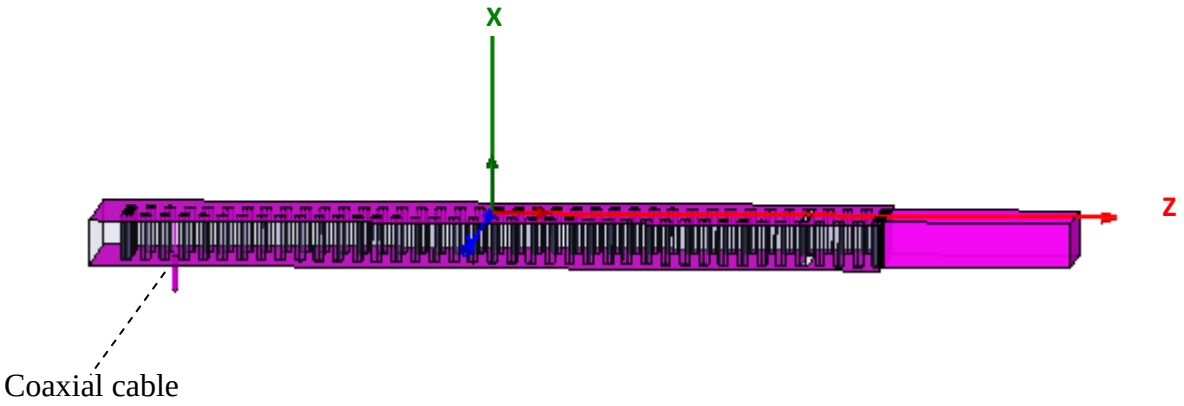

Figure 4.22 (b) another view

Dimensions of the antenna in Figure 4.22(a) are as follows:

Width of the slot (w_1) = 0.5 mm,

radius of the probe = 0.058 mm,

radius of the coax = 0.2 mm,

height of the probe = 2.5 mm,

flaring angle $\alpha = 3.179^0$,

thickness of the substrate 'h' = 3.175 mm, and

relative permittivity $\varepsilon_r = 2.2$ with loss tangent of 0.002.

The dimensions used for the modified horn slot antenna are used for this antenna; the dimensions of the coaxial cable are defined above. The comparison of the radiation pattern of the modified horn slot antenna with partial rectangular waveguide excitation and coaxial cable are shown in Figure 4.23. Good agreement has been observed for the radiation pattern in both the cases.

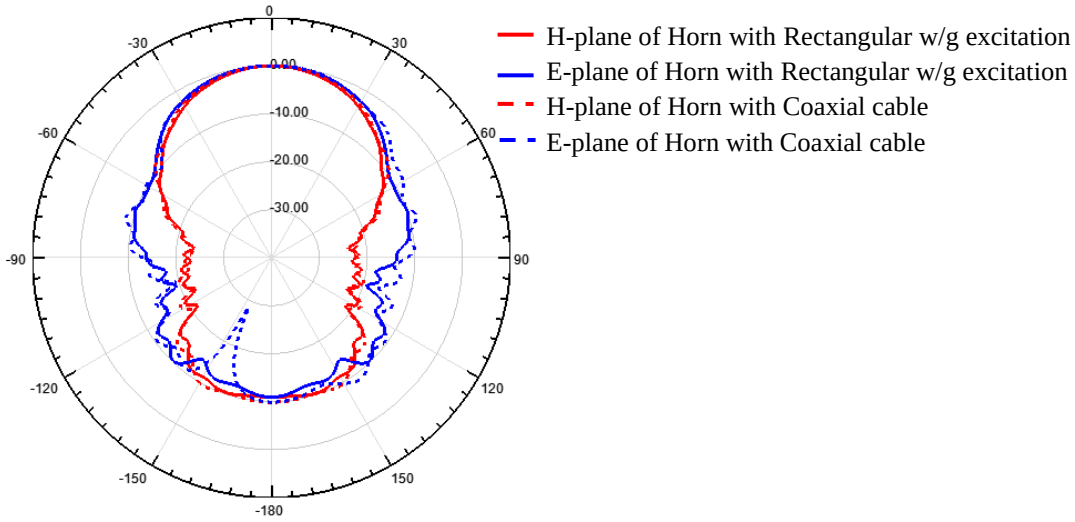

Figure 4.23 Comparison of far field radiation patterns for the horn excited using partial rectangular waveguide and coaxial cable at 23GHz

The comparison for reflection coefficient for both the cases is shown in Figure 4.24, where in both the cases a good matching is observed, which is below 15 dB. However, for the horn with the coaxial cable excitation, if the substrate is thicker (of 3.175mm) there is a chance of the existence of the higher order modes, so to avoid these higher modes we have tried to user thinner substrate.

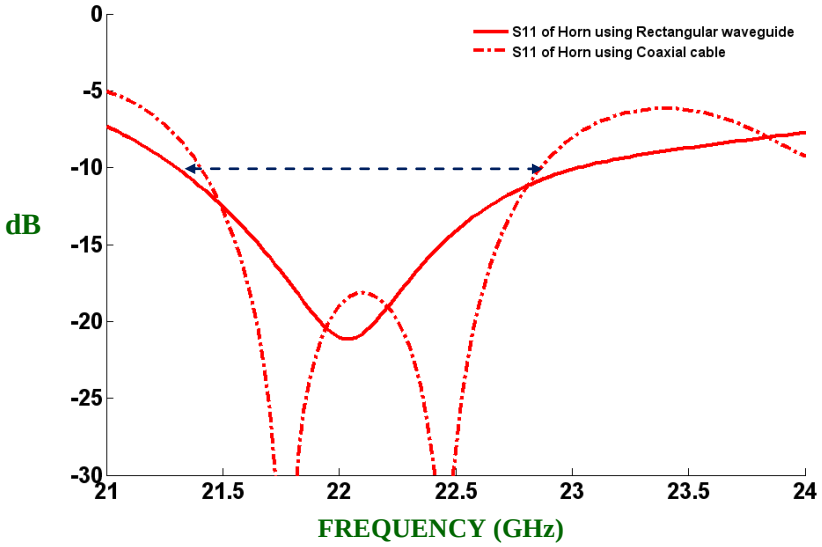

Figure 4.24 Comparison of reflection coefficient for the horn excited using partial rectangular waveguide and coaxial cable

When the substrate thickness is reduced to 1.57mm, a broadside radiation antenna is observed for the antenna as shown in Figure 4.25 (a), and a decrement in the bandwidth is also observed. The entire geometry is same, other than the slot width, which is optimized to 0.3mm to improve the matching. The comparison for the radiation pattern of the modified horn slot antenna with thinner substrate and thicker substrate is shown in Figure 4.25(b), where it is clear that the radiation patterns in both E-plane and H-plane became wider, despite of dielectric load at the aperture.

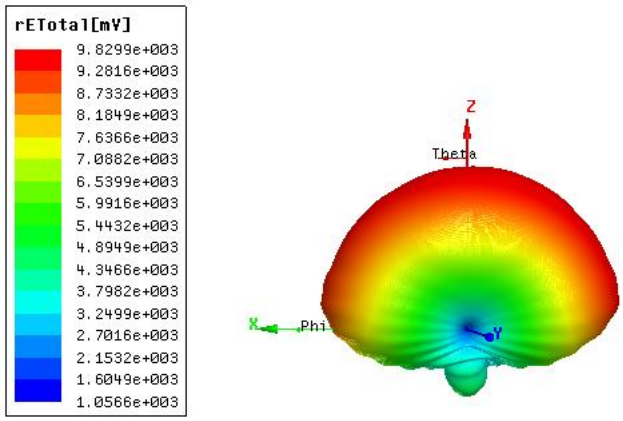

Figure 4.25 (a) 3-dimensional radiation pattern of the horn with thinner substrate at 23GHz

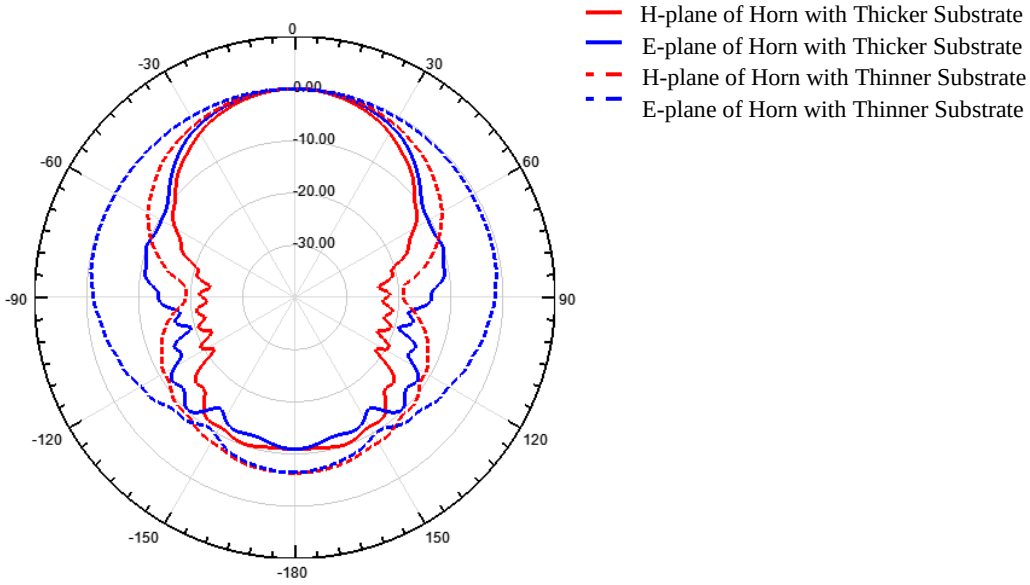

Figure 4.25 (b) Comparison of radiation patterns in both the planes for the horn with thicker substrate and horn with thinner substrate at 23GHz

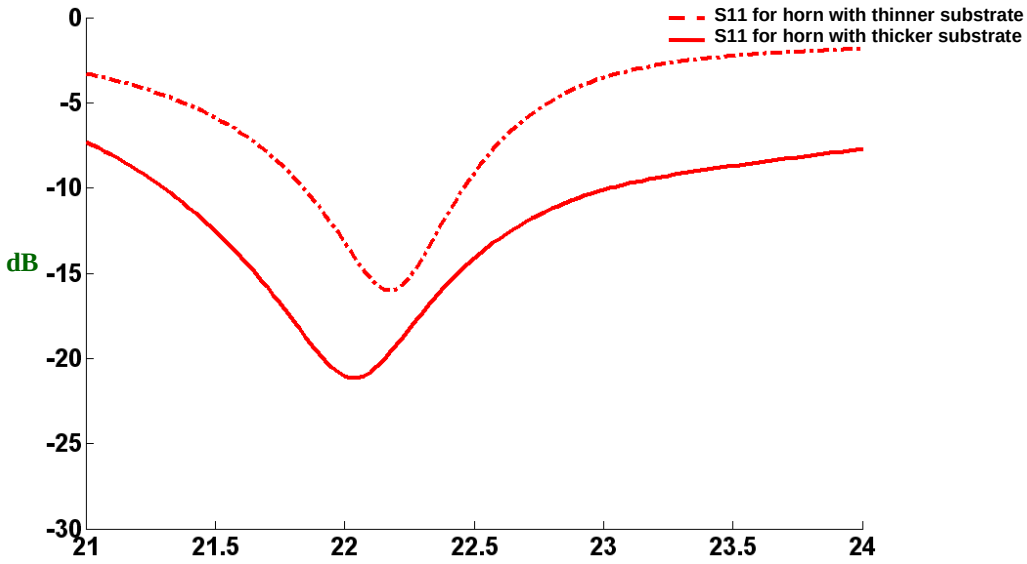

Figure 4.26 Comparison of reflection co-efficient for the horn with thicker substrate and horn with thinner substrate

Figure 4.26 depicts the comparison for reflection coefficient for both the cases, from which it can be observed that the reflection coefficient is increased by 3dB for this thinner case and the resonance is also shifted from 22GHz to 22.3GHz. Thus, it can be concluded that the thickness of the substrate affects both the radiation pattern and reflection coefficient. Finally, with this knowledge of the horn antenna we have tried to see the behavior of the antenna elements in the array environment which is discussed in the next chapter.

CHAPTER V

5.1. Antenna Array

The radiation characteristics of single-element antennas have been discussed and analyzed in the previous chapters. Generally, the radiation pattern of a single element is relatively wide, and each element provides low values of directivity (gain). For most antenna applications, antennas with high directive characteristics (high gains) are preferred to meet the demands of long distance communication. However, the directive characteristics can be accomplished by increasing the electrical size of the antenna and using dielectric load. Another way to enlarge the dimensions of the antenna, without necessarily increasing the size of the individual elements, is to form an assembly of radiating elements in an electrical and geometrical configuration. The new antenna, formed by using multiple elements, is referred to as an array. For most cases, the elements of an array are identical, which makes the array more convenient, simpler, and more practical. The elements of the array can be of various forms like wires, apertures, etc. The characteristic of the array can be controlled by the proper choice of the element (dipole, horn, patch, etc.), the geometry of the array, and the excitation (amplitude and phase) of the antenna.

The total field of the array can be computed by the vector addition of the fields radiated by the individual elements, assuming that the current distribution in each element is same as that of the isolated element. Usually, this is not the case; the current distribution in each element of the array depends on the separation distance between the elements. For the directive radiation

pattern of the array, the fields from the elements of the array interfere constructively (add) in the desired direction and interfere destructively (cancel each other) in the remaining space [14].

The five factors that affect the overall radiation pattern of an antenna are

i. Geometrical configuration of the array (linear, circular, rectangular, spherical, etc.)
ii. spacing between the elements
iii. excitation amplitude of the individual elements
iv. excitation phase of the individual element
v. radiation pattern of the individual antenna

With the knowledge of the antenna arrays we have tried to study and analyze the SIW horn antenna in the array environment. In this work, the antenna array is analyzed with the thicker substrate and the thinner substrate, with a design criterion of minimum side lobe level at a fixed main beam width and good matching.

5.2. SIW modified horn slot antenna array

In the previous chapter we have discussed different cases of an SIW horn antenna, and then concluded with the modified horn slot antenna. Here, we made an attempt to observe and study the behavior of the antenna in the array environment. An SIW antenna array formed by four dielectric loaded modified SIW horn slot elements is shown in Figure 5.1. The dielectric loaded SIW horn element can be integrated in the array easily [15]. Generally, resonant arrays of longitudinal slots in the broad wall of rectangular waveguides have the added advantage of very low cross-polarization levels. We have tried to extend this idea to SIW horns in this work, considering their relative simplicity in nature, ease of tuning to achieve desired radiation pattern

and their matching properties. Initially, we have tried to use the partial rectangular waveguide excited by a wave port, and after optimizing the structure we have tried to excite it using coaxial cable. As discussed earlier, thickness of the substrate plays a vital role in the antenna performance. Thus, we have started with the thicker substrate and concluded with the thinner substrate to avoid the propagation of higher order modes. The electric field distribution for the antenna array is shown in Figure 5.2, and single mode propagation is observed. The separation distance between the elements plays a vital role in reducing the sidelobe levels of the array.

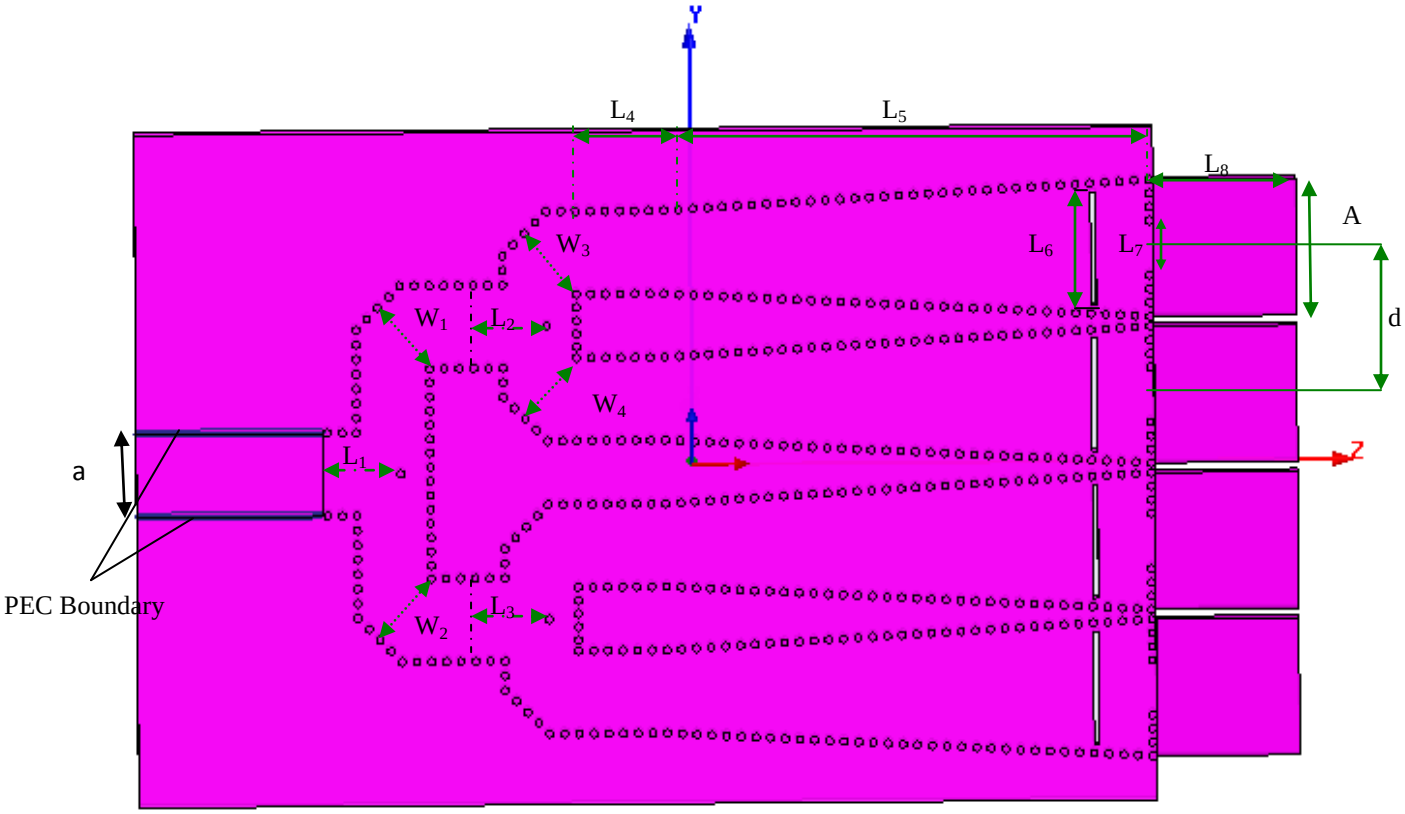

Figure 5.1 1×4 Dielectric loaded modified horn slot antenna array

Dimensions for the antenna array shown in Figure 5.1 are as follows:

Port width ‘a’ = 7mm,

radius of the via ‘r’ = 0.3875 mm,

separation between vias (center-center) ‘s’ = 1.37 mm,

$L_1 = L_2 = L_3 = 6.83$ mm,

$W_1 = W_2 = W_3 = W_4 = 6.8325$ mm, $L_4 = 9.607$ mm & $L_5 = 43.919$ mm,

length of the slot (L_6)= 10.62 mm($1.1*\lambda_g$),

length of the small aperture (L_7)= 5.23 mm($0.56*\lambda_g$) and spacing between the slots is 3.918 mm,

width of the slot = 0.5 mm,

length of the lens (L_8) = 13.32 mm,

aperture length(A) = 12.8 mm,

spacing between the elements (d) = 12.8 mm,

flaring angle $\alpha = 3.179^0$,

thickness of the substrate ‘h’ = 3.175 mm, and

relative permittivity $\varepsilon_r = 2.2$ with loss tangent of 0.002.

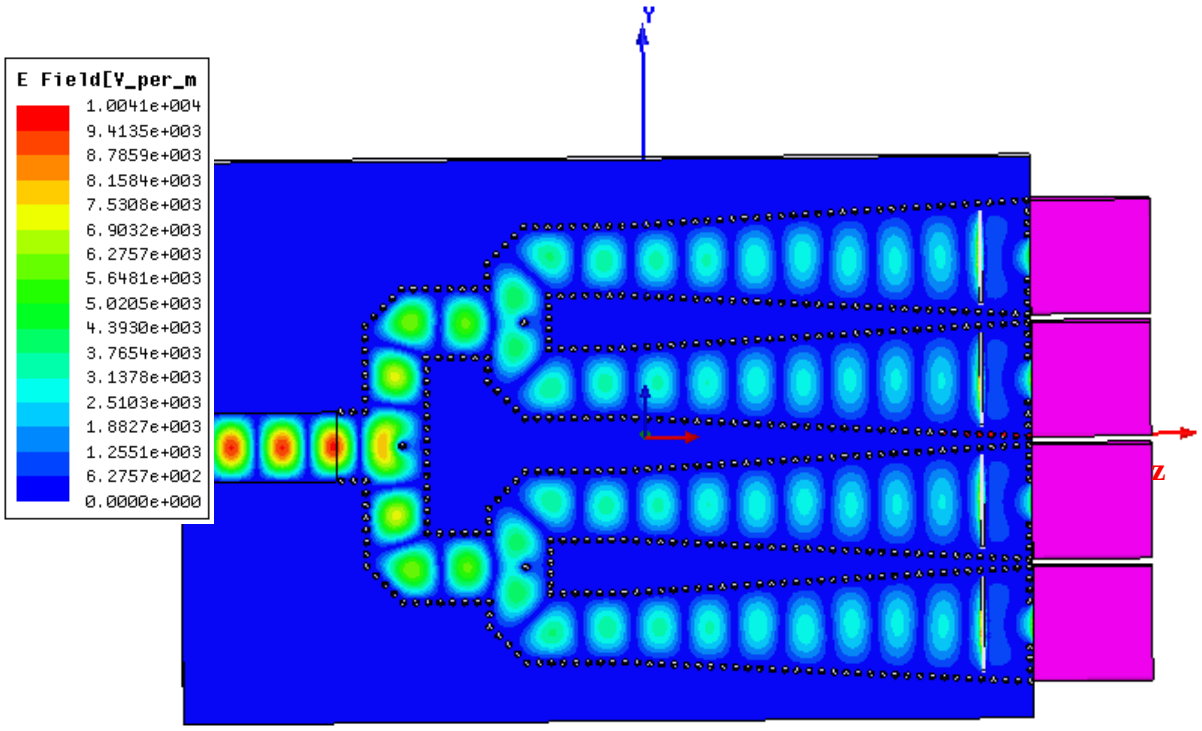

Figure 5.2 Electric field distribution of the 1×4 array

From Figure 5.2 the TE_{10} mode is forced to propagate because of the partial waveguide (higher order modes are avoided); equal power division can be observed for each 1:2 to power divider. The 3-dimensional radiation pattern of the array is shown in Figure 5.3. Here, the spacing between the elements is 12.8 mm which is less than a wavelength. It has been observed that the radiation pattern of the array is frequency dependent. As the frequency decreases the grating lobes move away from the visible region main beam, while as the frequency increases the grating lobes come closer to the main beam.

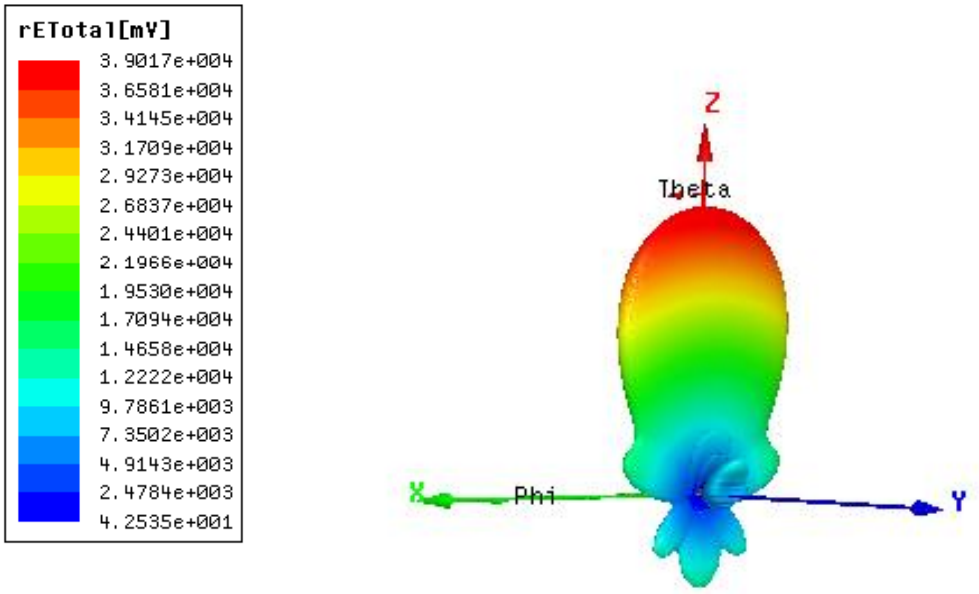

Figure 5.3 Three-dimensional radiation pattern of the 1×4 array at 23 GHz

The far field radiation patterns for the array along with the radiation pattern of the single element at 23GHz are shown in Figure 5.4; it can be observed that when the radiation pattern of the single element is multiplied by the array factor, which is function of frequency (k) and separation distance between elements (d), the sidelobes of the array in the H-plane are suppressed. For instance, at $\theta = 25^0$, the radiation pattern of the single element in the H-plane is of -2 dB and after array multiplication, the side lobes of the array are suppressed to - 12 dB.

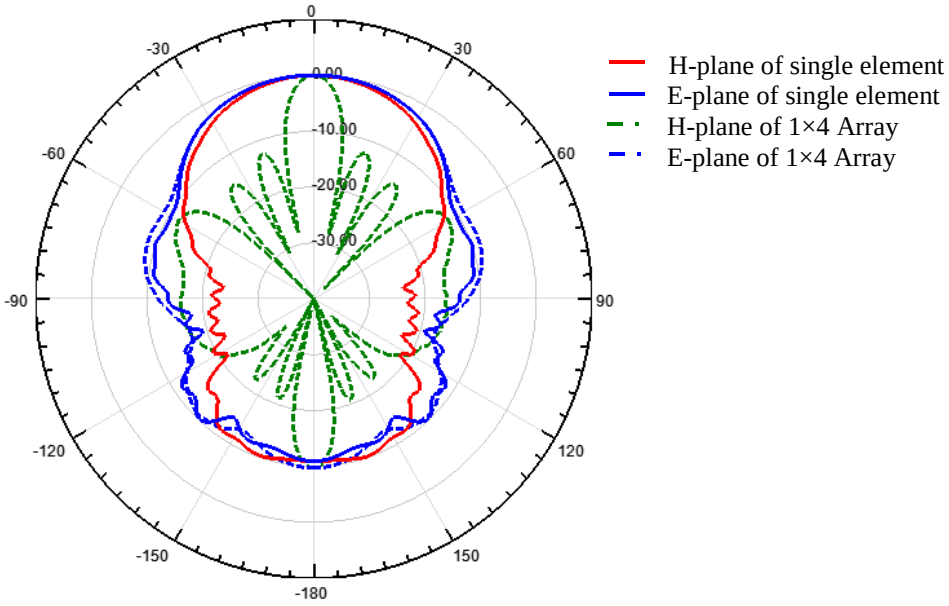

Figure 5.4 Radiation pattern of the 1×4 array at 23 GHz

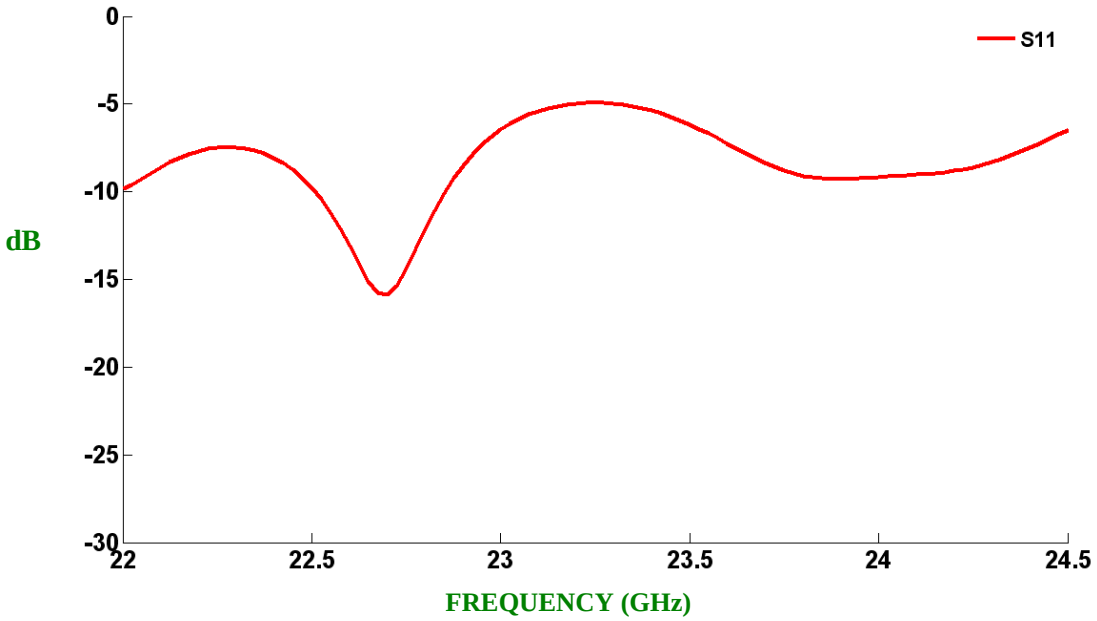

Figure 5.5 Reflection coefficient for the 1×4 array

Thus, for an 1×4 dielectric loaded modified horn slot antenna array, sidelobes of less than -12 dB and a back lobe of 8 dB are achieved. If the spacing between the elements is greater than one wavelength, undesirable grating lobes can be observed in the radiation pattern of the array. The reflection coefficient for the array is shown in Figure 5.5, a good matching is observed for a narrow band.

5.3. SIW modified horn slot antenna array fed by coaxial cable

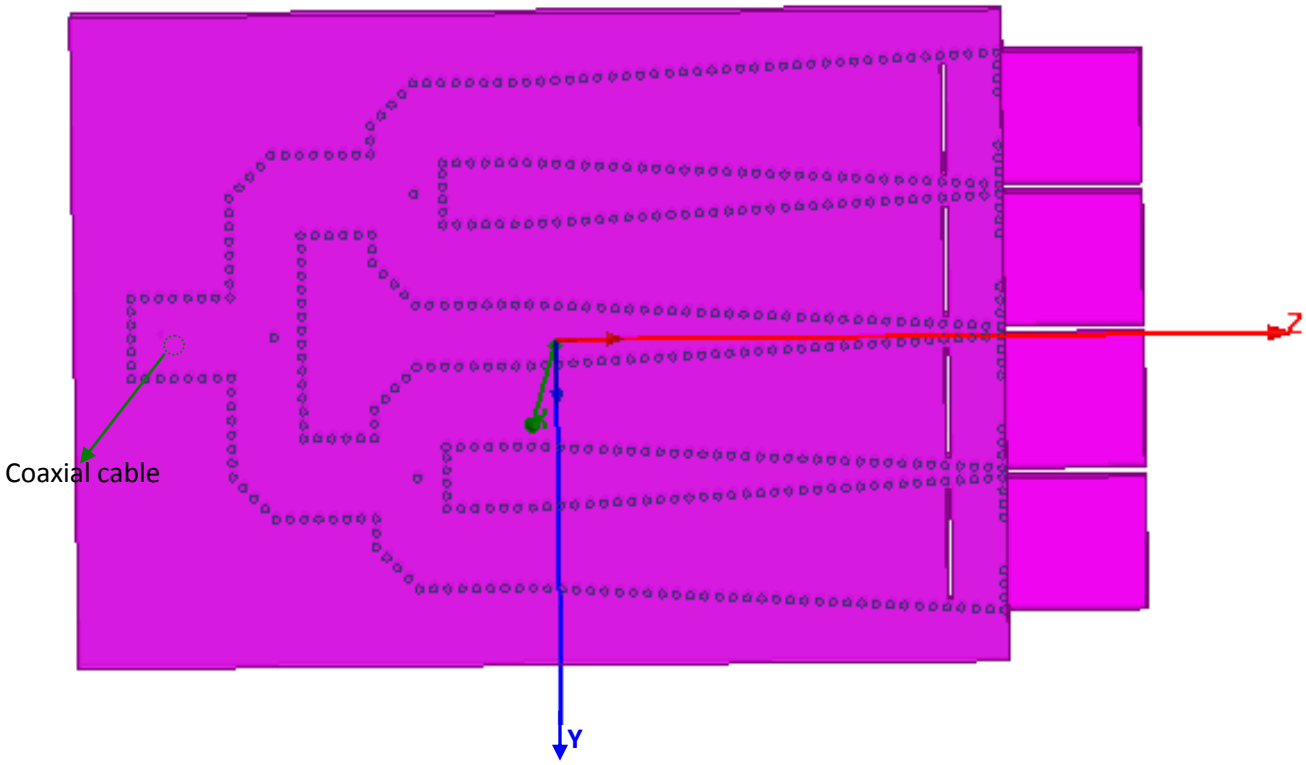

Figure 5.6 1×4 dielectric loaded modified horn slot antenna array fed by coaxial cable

Dimensions for the antenna array shown in Figure 5.6 are as follows:

Width of the slot = 0.5 mm,

radius of the probe = 0.058 mm,

radius of the coax = 0.2 mm,

height of the probe = 2.5mm,

flaring angle $\alpha = 3.179^0$,

thickness of the substrate 'h' = 3.175 mm, and

relative permittivity $\varepsilon_r = 2.2$ with loss tangent of 0.002.

Practically, the partial rectangular waveguide cannot be used for measurements, so we have tried to use coaxial cable of 50 Ohms for the excitation. The geometry of the 1×4 antenna array, excited by coaxial cable is shown in Figure 5.6; the opening of the waveguide is closed by the wall of vias, keeping all the other dimensions the same. The comparison for the radiation pattern for the 1×4 antenna array using partial rectangular waveguide and coaxial cable is shown in Figure.5.7.

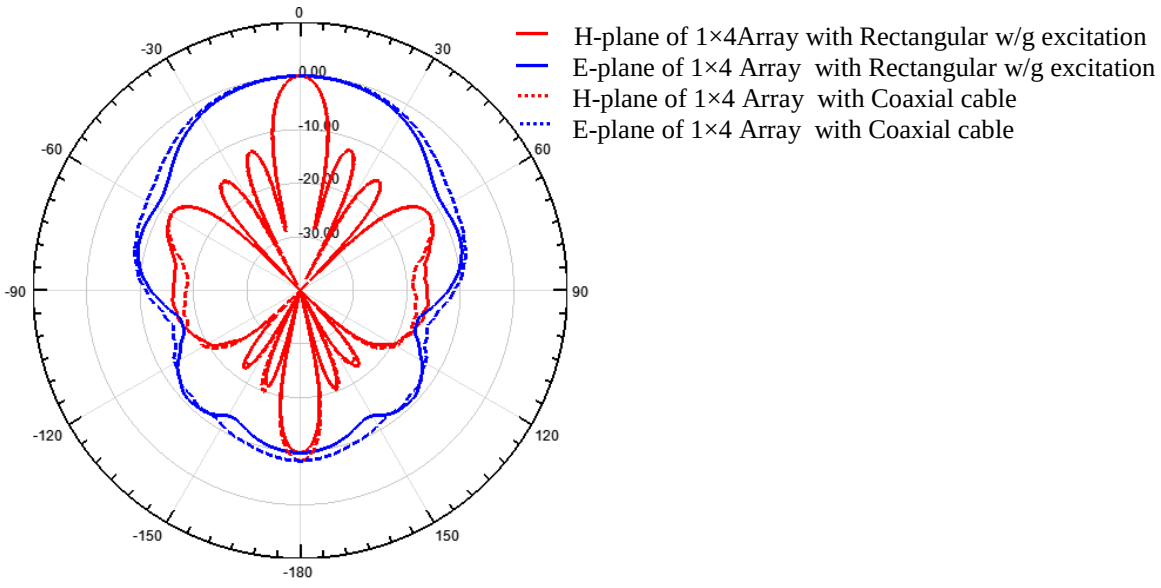

Figure 5.7 Comparison of radiation patterns in both the planes for the 1×4 array excited using partial rectangular waveguide and coaxial-cable at 23GHz

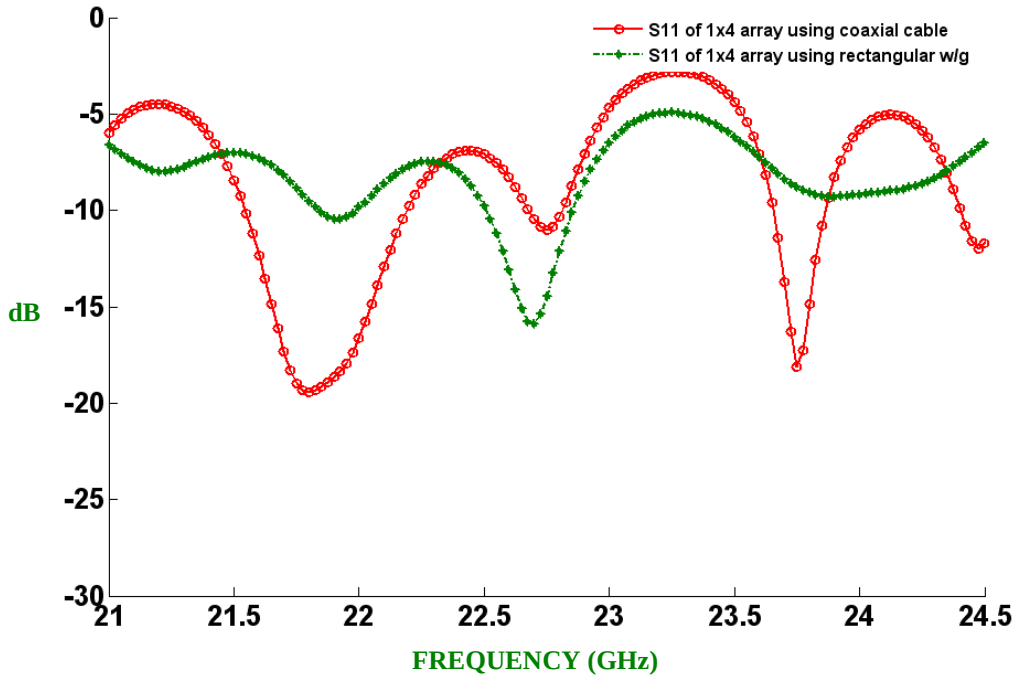

Figure 5.8 comparison of reflection coefficient for the 1×4 antenna array using coaxial cable and partial waveguide excitation

From Figure.5.7, a good agreement for both the cases can be observed. The comparison for reflection coefficient of the array excited by a coaxial cable and partial rectangular waveguide is depicted in the Figure 5.8. The dimensions of the coaxial pin and probe can be optimized to achieve good matching for the array. This 1×4 dielectric loaded modified horn slot antenna array can next be extended to a 1×8 antenna array.

Since the geometry consists of 307 metallic vias for 4 elements, the simulation software HFSS takes lot of time for the synthesis of the structure. If we have 8 elements, it consumes more time. To reduce computation time two model simplifications can be implemented:

i. line of symmetry

ii. vias can replaced by the metallic solid walls

5.4. 1×8 Antenna Array using Metallic Solid walls

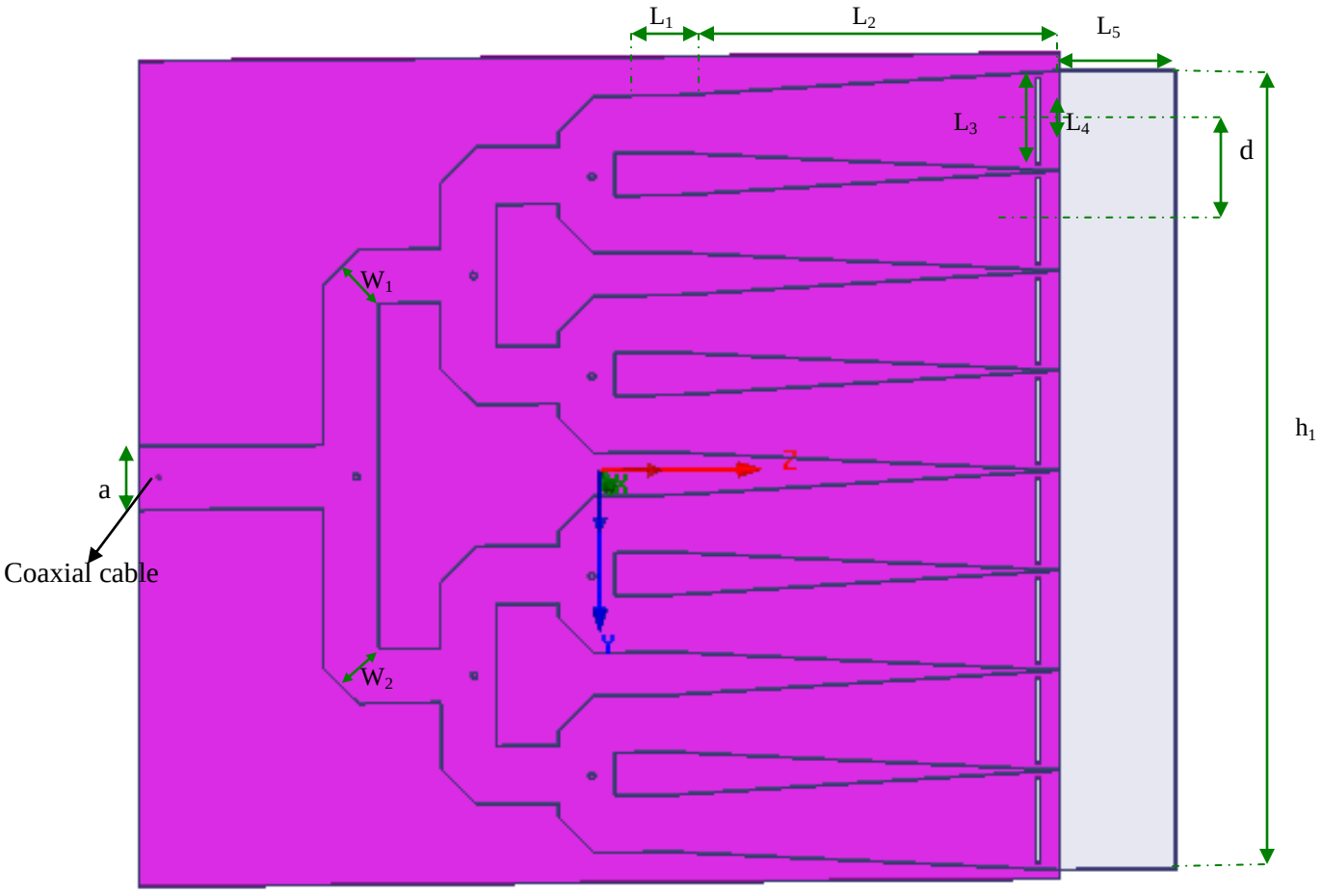

Figure 5.9 1×8 antenna array using metallic solid walls

Dimensions for the antenna array shown in Figure.5.9 are as follows:

Port width ‘a’ = 7.3 mm,

W_1 =,W_2 = 6.8325 mm,

L_1 = 9.607 mm,

L_2 = 43.919 mm,

length of the slot (L_3)= 10.62 mm($1.1*\lambda_g$),

length of the small aperture (L_4)= 5.23 mm($0.56*\lambda_g$),

spacing between the slots = 3.918 mm,

width of the slot = 0.5 mm,

length of the lens (L_5) = 13.32 mm,
height of the lens (h_1) = 102.4 mm,

spacing between the elements (d) = 12.8 mm

radius of the probe = 0.058 mm,
radius of the coax = 0.2 mm,

height of the probe and coax = 2.5mm
thickness of the substrate ‘h’ = 1.57 mm, and

relative permittivity ε_r = 2.2 with loss tangent of 0.002,

In order to reduce the computation time for 8 elements, the metallic vias of the array are replaced by the solid metallic walls as shown in Figure 5.9. A thinner substrate is used for the modeling of the 1×8 Antenna Array (to avoid the propagation of higher order modes). The array is excited by a 50Ω coaxial cable and the dimensions of the coaxial cable have been optimized to improve matching. The 3-Dimensional radiation pattern is shown in the Figure 5.10 (a), where a wider main beam can be observed. The radiation patterns in the H-plane and E-plane are depicted in Figure 5.10 (b). Sidelobe levels of less than -12 dB and a high back lobe radiation is obtained. This high back lobe radiation may be because of the element pattern and also the chosen frequency band.

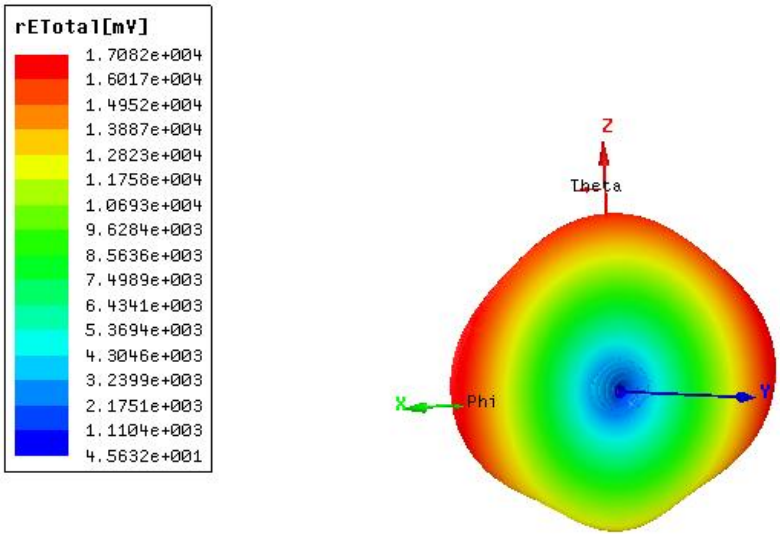

Figure 5.10 (a) 3-dimensional radiation pattern of the array at 23GHz

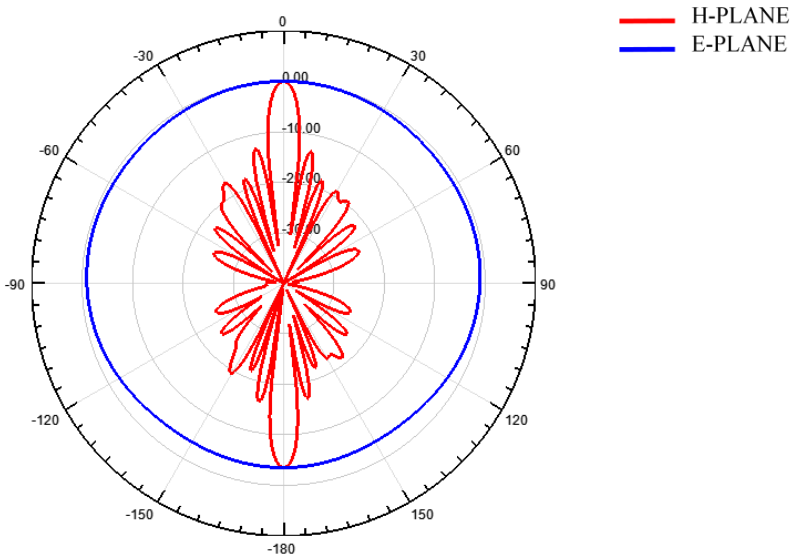

Figure 5.10 (b) radiation patterns in both planes of the 1×8 solid wall antenna array at 23GHz

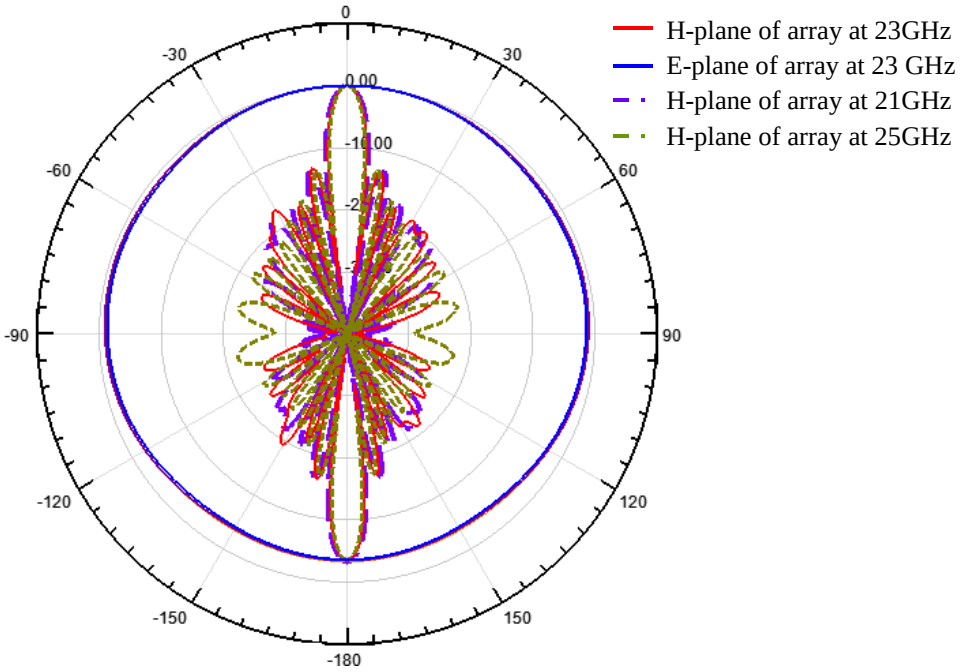

Figure 5.11 radiation patterns in both the planes of the 1×8 solid wall array at different frequencies

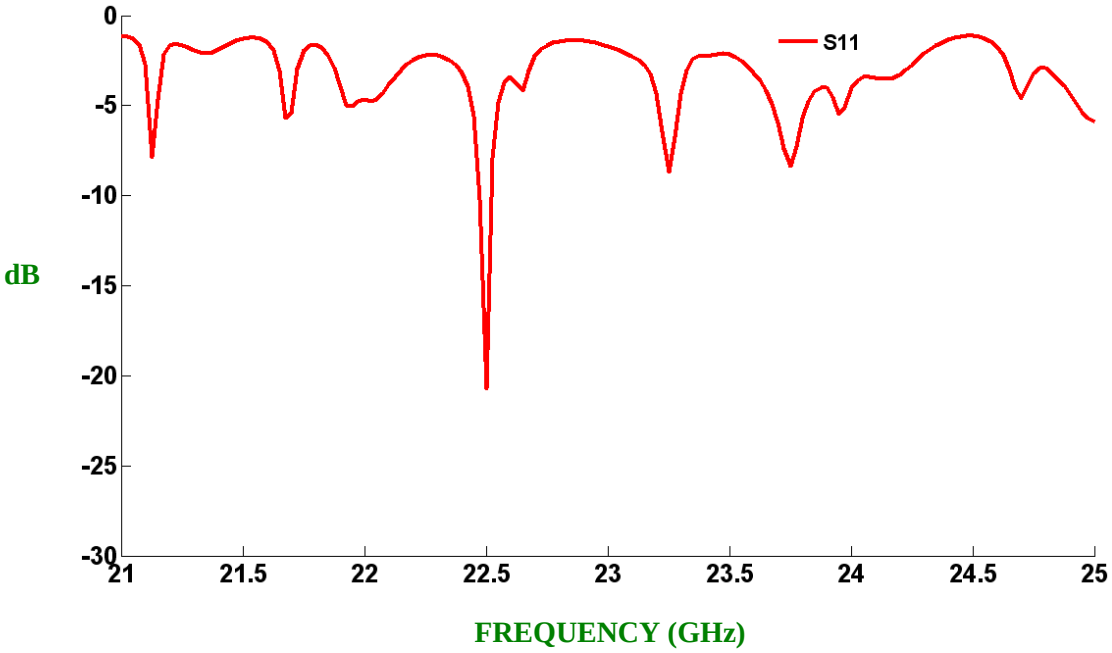

Figure 5.12 Reflection coefficient of the 1×8 array

Radiation patterns for the 1×8 dielectric loaded modified horn slot antenna array for different frequencies are shown in Figure 5.11. It has been observed that the radiation pattern of the array is frequency dependent, and that as the frequency decreases, e.g., at 21 GHz grating lobes move away from the visible region of the main beam, while as the frequency increases e.g., at 25 GHz the grating lobes come closer to the main beam. The reflection coefficient of the array is shown in Figure.5.12. Matching for only a narrow bandwidth is achieved due to the thickness of the substrate.

5.5. EM Co-simulation approach to the Antenna Array

The EM Co-simulation technique can be extended to the antenna array in order to save computation time. The Co-simulation approach extended to the 1×4 antenna array is elaborated on the block diagram shown in Figure 5.13. Here, ADS is the circuit simulator and HFSS simulation software is the EM simulator.

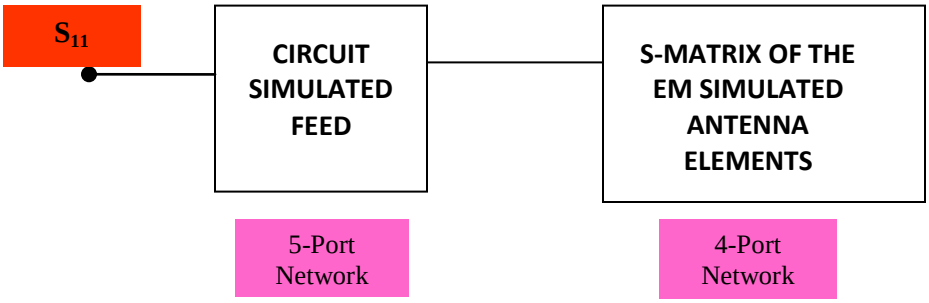

Figure 5.13 Block diagram explaining co-simulation approach to the 1×4 array

In order to understand this approach in a better way we considered an example of 1×4 modified horn slot antenna array as shown in Figure 5.14. To implement this technique, as a first step the feed for the array is designed by assembling T-junctions and bends using a circuit simulator, which is nothing but a 5-port network, as indicated in the block diagram. Thus, the scattering matrix for the feeding network is obtained.

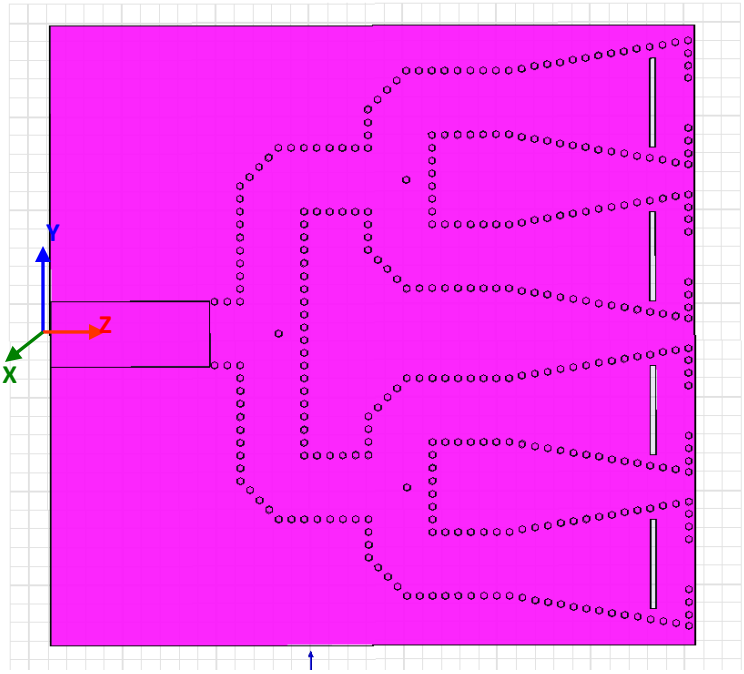

Figure 5.14 1×4 modified horn slot antenna array

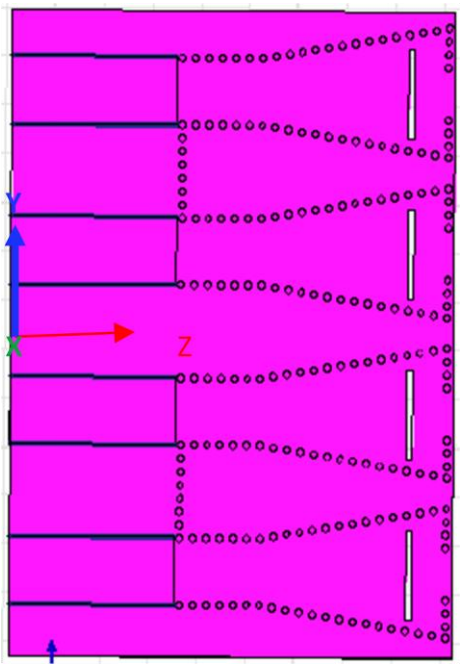

Figure 5.15 Antenna array modeled using EM simulator

For the second step we model an array of 4 elements with coupling as shown in Figure 5.15 using an EM simulator. In this model, each element is excited individually, preserving the

mutual coupling between the antenna elements, which is nothing but a 4-port network. Thus, the EM simulated scattering matrix for the antenna elements is obtained. These S-matrices for the feeding network and antenna elements are then assembled using the circuit simulator as indicated in the block diagram, and S_{11} for the 1×4 array can be obtained as shown in the block diagram.

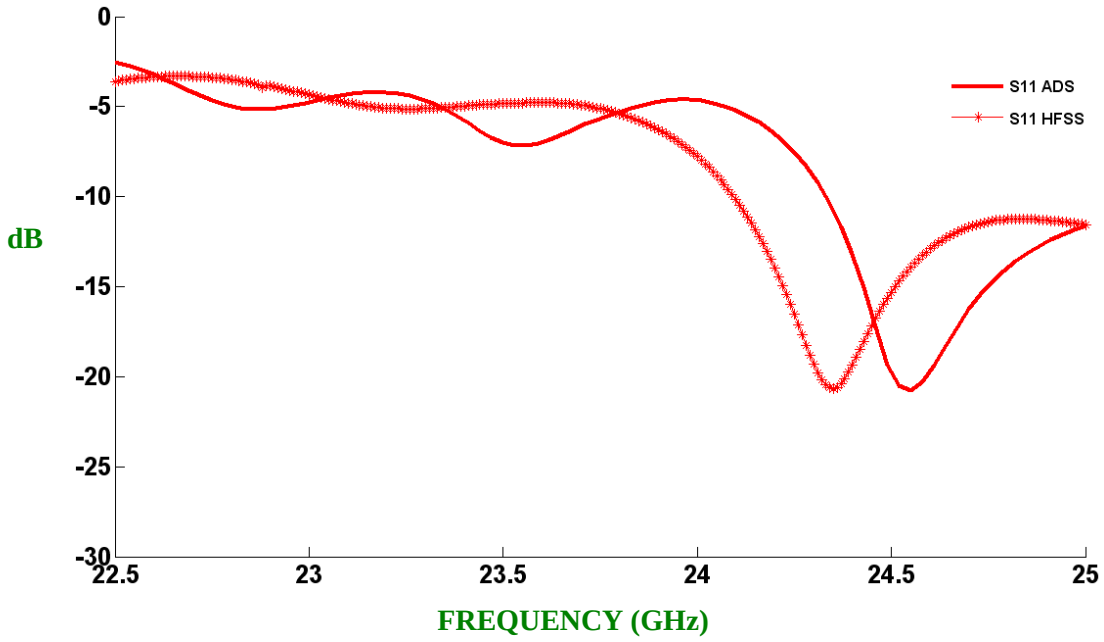

Figure 5.16 Validation for the reflection coefficient

Table 5.1 Comparison of the Simulation Time

SOFTWARE	MEMORY	TIME (minutes)
ADS	320GB, 1 GB RAM	1.2
HFSS	320GB, 1 GB RAM	79

The validation for the reflection coefficient from the 1×4 antenna array using the co-simulation technique and HFSS simulation software is shown in Figure 5.16, a small discrepancy is observed. The comparison for the simulation time is shown in Table 5.1, where a great reduction in the computation time is observed while comparing to full wave analysis.

CHAPTER VI

6.1 Conclusions

In this work, the concept of Substrate Integrated Waveguide (SIW) was realized by using two rows of metallic vias to simulate side walls of a rectangular waveguide in a dielectric substrate. Also, C++ code based on the method of moment and cylindrical wave expansion referred to as a Hybrid Method have been studied, which can be used to design passive devices such as feeding networks, filters, directional couplers, isolators, etc. In order to ensure the propagation of the TE_{10} mode, a partial waveguide having PEC boundary on the two walls of the waveguide was studied and implemented. A 1:8 power divider feeding network using the C++ code and HFSS simulation software was designed and compared for a narrow bandwidth. When the simulated S-parameters for both cases were compared, even though they followed the same trend a small discrepancy was found and this discrepancy were believed to be due to the number of segments used for the regular polyhedron of the HFSS. Later, a solid wall feeding network was modeled, replacing metallic vias with the metallic solid walls, which reduced the computation time, and provided an opportunity to study the equivalence between the SIW and conventional waveguide.

The EM circuit Co-simulation technique was studied and implemented for the feed as well as the antenna array. In this approach, the passive components such as T-junction, bend and a waveguide are synthesized and analyzed within less time are compared to a finite

element solution. When the co-simulated S-parameters were compared with the EM simulated S-parameters, they followed the same trend with a small discrepancy.

Initially, our goal was to design an SIW horn antenna several problems were encountered and efforts were made to overcome the problems in design. In the process, an SIW horn with dielectric load, an SIW horn with a slot on one side of the horn (upper PEC), an SIW horn with a reflection cancelling slot pair, and an SIW horn with a slot with a small opening in the aperture were studied and then we concluded with the modified horn slot antenna with slots on both sides of the horn (top and bottom PEC sheets). SIW horn, with the partial waveguide excited by a wave port and a 50 Ω coaxial cable excitation were analyzed and compared. Later on the metallic vias were replaced by the metallic solid walls in order to reduce the computation time; both the cases were compared and a good agreement was found. Then a 1×4 SIW horn antenna array using metallic vias was modeled and sidelobes of -12 dB level were achieved. Finally 1×8 antenna arrays were modeled using metallic solid walls to reduce the computation time.

6.2. Future Work

It is believed that an effort can be made to reduce the side lobe levels, as well as the matching of the 1×8 antenna array can be improved. Now that we have 1×8 array geometry, the metallic solid walls can be replaced by metallic vias for SIW antenna array. This array can be extended to design an 1×16 array, also can be measured practically.

REFERENCES

[1] X. Xu, R. G. Bosisio, and K. Wu, “A new six-port junction based on substrate integrated waveguide technology," *IEEE Trans. Microwave Theory Tech.*, vol. 53, July 2005 pp. 2267-2273.

[2] Wenquan Che, Lei Xu, Dapeng Wang, Liang Geng, Kuan Deng, and Y. L.Chow, “Equivalence between Substrate-Integrated (SIRW) Rectangular waveguide short-circuit load and its equivalent rectangular waveguide short-circuit load," *IEEE Microwave and Optical Technology Letters*, Sep. 2006 , vol. 48, No.9, pp. 1694-1698.

[3] W.-Q. Che, C.-X. Li, D.-P. Wang, and L. Xu, “Investigation on the Ohmic Conductor Losses in Substrate Integrated Waveguide and Equivalent Rectangular Waveguide,” *Journal of Electromagnetic Waves and Applications*, Volume 21, No.6, Nov. 2007, pp. 769-780.

[4] X. H.Wu and A. A. Kishk, “Hybrid of Method of Moments and Cylindrical Eigenfunction Expansion to Study Substrate Integrated Waveguide Circuits," *IEEE Trans. Microwave Theory and Techniques*, vol. 56, Aug. 2008, pp. 2270-2276.

[5] Wenquan Che, Edward Kai-Ning Yung, and Ke Wu, “Millimeter-wave substrate integrated waveguide ferrite phase shifter for wireless communication application,” *Wireless Communication Technology, IEEE Topical Conference*, Aug. 2004, pp. 320-324.

[6] Rohit Sammeta**,** “Substrate integrated waveguide slot array antenna and its numerical analysis,” Department of Electrical Engineering, May 2007.

[7] Feng Xu and Ke Wu , “Guided-wave and leakage characteristics of substrate integrated waveguide,“ *IEEE Trans. Microwave Theory and Techniques*, vol. 53,no.1, Jan. 2005, pp 66-73.

[8] Xuan HuiWu and Ahmed A. Kishk, “Analysis and Design of Substrate Integrated Waveguide Using Efficient 2D Hybrid Method, “ 2010.

[9] Ke Wu, Dominic Deslandes, and Yves Cassivi, “The Substrate Integrated Circuits - A New Concept for High-Frequency Electronics and Optoelectronics," *Telecommunications in Modern Satellite, Cable and Broadcasting Service, TELSIKS 6th International Conference*, vol. 1, Nov. 2003, pp. III-X.

[10] Smith, N. A. and R. Abhari, “Compact substrate integrated waveguide wilkinson power dividers," *IEEE Antennas and Propagation Society International Symposium*, July 2009, pp. 1-4.

[11] ZhargCheng Hao, Wei Hong, Hao Li, Hua Zhang, Ke Wu, “Multiways Broad Substrate Integrated Waveguide (SIW) Power Divider," *IEEE Antennas and Propagation Society International Symposium*, Vol. 1A, Dec. 2005, pp. 639 - 642.

[12] Simon Germain, Dominic Deslandes and Ke Wu,“Development of substrate integrated waveguide power dividers,“ *IEEE CCECE*, vol.3, pp. 1921-1924, May 2003.

[13] Sanghoon Shin and Sridhar Kanamaluru,“Diplexer design using EM and circuit simulation techniques," *IEEE Trans. Microwave Theory and Techniques*, vol. 8, pp. 77-82, April 2007.

[14] C. Balanis, *Antenna Theory*, 2nd ed. New York: Wiley, p. 651.

[15] H. Wang, D. G. Fang, B. Zhang and W. Q. Che, “Dielectric Loaded Substrate Integrated Waveguide (SIW) H-Plane Horn Antennas," *IEEE Trans. Antennas and Propagation*, vol. 58, no. 3, pp. 640–647, Mar. 2010.

[16] Wong, M. Sebak, A.R. Denidni, T.A, “A Broadside Substrate Integrated Horn Antenna,” *IEEE Antennas and Propagation Society International Symposium*, pp. 1-4, Sep. 2008.

[17] Bo Pan, Yuan Li, George E. Ponchak, John Papapolymerou, and Manos M. Tentzeris, "A 60-GHz CPW-Fed High-Gain and Broadband Integrated Horn Antenna," *IEEE Trans. Antennas and Propagation*, vol. 57, no. 4, pp. 1050 – 1056, April. 2009.

[18] Sakakibara, K. Hirokawa, J. Ando, and M. Goto, N. "A slotted waveguide array using reflection-cancelling slot pairs," *IEEE Antennas and Propagation Society International Symposium*, Vol. 3, pp. 1570 – 1573, Dec. 2005.

[19] Li Yan, Wei Hong, Guang Hua, Jixin Chen, Ke Wu, and Tie Jun Cui, "Simulation and Experiment on SIW Slot Array Antennas," *IEEE Microwave and Wireless Components Letters*, vol. 14, no. 9, Sep. 2004.

[20] Demir, S, "Dielectric Antenna array feed network topology determination with frequency bandwidth considerations," *IEEE Antennas and Propagation Society International Symposium*, vol. 3, pp. 940–945, Aug. 2003.

[21] Sammeta. R, Reddy, C.J, Glisson. A, Kishk.A, "A Substrate Integrated Waveguide Slot Array Antenna Fed with a Grounded Coplanar Waveguide," *IEEE Antennas and Propagation Society International Symposium*, pp. 1-4, Sep.2008

[22] The Basics of Antenna Arrays by G.J.K Moernaut and D. Orban, Orban Microwave Products www.orbanmicrowave.com.

[23] W. L. Stutzman and G. A. Thiele, *Antenna theory and Design*, 2nd ed., John Wiley & Sons, 1998.

[24] HFSS, Ansoft Corporation Version 11, Copyright 2006.

VITA

B.TECH in ELECTRONICS AND COMMUNICATION (2003-2007) from Jawaharlal Nehru Technological University, India.